An Experimental Study of Worthington Jet Formation After Impact of Solid Spheres

by

Jenna Marie McKown

B.S., Mechanical and Ocean Engineering
Massachusetts Institute of Technology (2010)

Submitted to the Department of Mechanical Engineering
in partial fulfillment of the requirements for the degree of

Master of Science in Ocean Engineering

at the

MASSACHUSETTS INSTITUTE OF TECHNOLOGY

June 2011

Author .....
Department of Mechanical Engineering
May 6, 2011

Certified by .....
Alexandra H. Techet
Associate Professor of Mechanical and Ocean Engineering
Thesis Supervisor

Accepted by .....
David Hardt, Professor of Mechanical Engineering
Chairman, Department Committee on Graduate Theses

An Experimental Study of Worthington Jet Formation After Impact of Solid Spheres

by

Jenna Marie McKown

Submitted to the Department of Mechanical Engineering
on May 6, 2011, in partial fulfillment of the
requirements for the degree of
Master of Science in Ocean Engineering

Abstract

The impacts of solid spheres with the free surface have been studied for over one hundred years. In this thesis, the Worthington jets resulting from the impacts of hydrophobic and hydrophilic spheres with the free surface are studied experimentally. Several impact velocities and three materials of differing mass ratios are used. The resulting jets are characterized in terms of common non-dimensional physical parameters. A single camera is used to image activity both above and below the free surface simultaneously. The resulting images provide measurements of the height and velocity of the Worthington jets, as well as information about the breakup of the columns of fluid into droplets.

In the hydrophilic cases, two separate regimes of jet formation are observed. The heights of both the first and second jet are recorded with time, and the maximum heights of each jet are compared to the Froude number at impact. The maximum height of the second jet is found to scale linearly with We, which is calculated using the velocity of the jet tip rather than impact velocity. Viscosity is shown to be negligible while a dependence on gravity is indicated. The time at which the first jet breaks up is proportional to Froude number, while the time of breakup for the second jet is nearly constant. Comparisons to energy transfer are presented.

In the hydrophobic cases, the Worthington jet results from the collapse of the cavity formed below the free surface. Heights of the continuous Worthington jet are recorded for each time step, and average maximum heights obtained are again compared to Froude and Weber numbers. The increased variability in these data hinder clear scaling, and experimental error is calculated from repeated trials of two representative cases. Unaffected by experimental variation, however, the lifespan of the Worthington jets is shown to depend linearly on Froude number. Energy comparisons are explored.

Thesis Supervisor: Alexandra H. Techet
Title: Associate Professor of Mechanical and Ocean Engineering

Acknowledgments

This thesis would not have been possible without my advisor, Alexandra Techet, who has mentored and supported me throughout my time at MIT. Her words of encouragement and advice kept me focused through this whirlwind of a Masters program. I am ever grateful for the confidence that she had in me, despite my intermittent lack of confidence in myself.

Tadd Truscott was instrumental to the completion of this thesis, providing endless enthusiasm and encouragement, and helping me get as excited about the research as he is... well, almost. On the really slow days when I didn't much feel like working, it was Jesse Belden who always seemed to give me the extra drive I needed to keep at it, mostly because his work ethic would make anyone feel like a slacker. Tadd, Jesse, and Brenden Epps, my UROP supervisor way back when, all helped introduced me to this lab and showed me the ropes. Anna Shih was excellent for distracting me when I most needed it, and sometimes when I didn't. But I'm sorry that all of her fish died on my watch. Shmu and Jeff were my support team upstairs, giving me endless support.

My family has been extremely supportive, listening to me whine and complain, and also putting up with my insane propositions of quitting school and becoming a boat bum in the British Virgin Islands... I didn't think my mother would steal my idea and do it first. I would not have been able to stay sane if it weren't for their constant reminders not to worry so much and to have fun.

This thesis is brought to you by the letter W, and the number 2.

Contents

List of Figures

List of Tables

Chapter 1

Introduction

The impact of solid spheres with the free surface has been studied for over one hundred years, and throughout that time, the upward-projecting jet that erupts from the place of impact has been of high interest to hydrodynamicists. The dynamics of water entry and the resulting cavity have been well defined theoretically, as well as extensively proven experimentally. Only recently, however, has the jet, known as the "Worthington jet," come under close examination.

Worthington jets can reach significant heights, typically much higher than the position from which an impacting solid sphere was released. The characteristics of the jet vary greatly depending on several factors, including the surface of the sphere and the impact velocity. Given that the Worthington jet is easily visible and recordable, a known relationship between the jet characteristics and the impact itself would provide invaluable information towards determining the conditions of an impact after-the-fact.

This thesis provides a link between the dynamics of solid sphere impacts and the characteristics of the resulting Worthington jet. The goal is to determine a simple scaling factor between the height from which the sphere is released and the ultimate maximum height of the continuous portion of the resulting Worthington jet. Jet breakup plays an important role in this determination, especially for the impact of hydrophobic spheres. Combining an understanding of the factors that drive the breakup process with information about the characteristics of the Worthington jet, a model can be produced that will aid in the prediction of Worthington jet height.

Also, the information about the breakup of the fluid jets can be extended to other problems in hydrodynamics, such as fluid jets in a crossflow of air.

In this study, the impacts and resulting Worthington jets of different spheres with hydrophilic and hydrophobic surfaces are recorded with high-speed photography. Several impact velocities, described by Froude number, and three materials of differing mass ratios are used. The resulting data are analyzed and a simple characterization of Worthington jet features using physical parameters at impact is proposed.

1.1 Review of Literature

1.1.1 Studies of Impacts

Photographs of sphere and drop impacts with the free surface have been taken and studied since Worthington's first experiments in the late 19th century [33]. Since then, there have been numerous studies on impacts and the resulting fluid dynamics. Splashes of liquid drops into liquids, solid objects into granular substrates, and solid objects into liquid pools of varying dimensions have been thoroughly examined, and many models for the resulting cavities and splash components presented.

Worthington began studying impacts by taking images of splashes with single-spark photography in the 1890s. His work revealed the difference between the impact of a smooth and that of a rough sphere with the free surface, and his experiments evaluated the transition between impacts that form cavities and those that don't, finding that even "polished," or hydrophilic, spheres produce cavities when dropped from a great enough height, while "rough," or hydrophobic, spheres always produce cavities [34].

This transition from smooth to rough splashes was further considered by Duez et al. in 2007. Through their own series of experiments with small spheres of different materials and surface treatments, they found the threshold impact velocity for cavity formation as a function of the contact angle of water with the sphere surface (a measure of the hydrophibicity). They also found that the threshold impact velocity

for completely hydrophilic spheres to form cavities is approximately $7.5m/s$ [10].

The results published by Duez were found in agreement with simulations performed by Do-Quang and Amberg, who varied the Reynolds and Bond numbers from the experiments by Duez and confirmed that the determining factor for cavity formation is dynamic wetting [9].

1.1.2 Experimental Variations

Depending on the individual interests of researchers, the splashing experiment has been altered to place emphasis on cavity formation [4, 3, 15, 22, 24, 2, 27], on the forces on the impacting object at impact [25, 27], and on the singularity at cavity collapse [5, 14, 19, 20, 36]. There is endless overlap in experimental methods, with various combinations of values of dimensionless quantities such as Bond number and Weber number, ensuring that the problem remain interesting to a large academic audience. Despite the many variations, the common focus on cavity dynamics, initial impact forces, and splash dynamics connects the interests of researchers across the board.

Droplet Impacts

In addition to solid spheres impacting water, impacts of small spheres and liquid drops have been studied by many [4, 12, 18, 23, 2]. Hsiao et al. determined a critical Weber number that divides liquid drops into two regimes: that in which there is little splash, accompanied by the creation of a vortex ring, and that in which there is a splash that results in a Worthington jet [18]. The vortex ring below the surface was found to be absent in cases where an upward jet was formed.

In the splashing regime, Fedorchenko and Wang did a study of the influence of viscosity and depth of the pool of liquid on the splash characteristics, forming models for the cavity, crown, and jet [12]. As one characteristic of the jet formation, Fedorchenko found that the jet velocity increases inversely to the vertex angle of the conical cavity formed by the drop [12]. Dependence on Froude number was also

shown, as well as a dependence on capillary length [12].

Ogawa also did a set of experiments to develop a theoretical model for the cavities and Worthington jets resulting from liquid drops impacting a surface of the same liquid [2]. These models focused on the maximum radius reached by the cavity and geometrical parameters of the jet, including maximum height. Newtonian solutions of water and glycerol were used along with non-Newtonian polymer solutions [2].

In the experiments conducted by Marston and Thoroddsen in 2008, the drop was of a different liquid and a higher viscosity than the pool it impacted. In this case, the drop does not coalesce into the liquid, but is enveloped by it. When the liquid reaches the apex of the viscous drop, the jet is formed, and was found to have a velocity more than 10 times the velocity of the impacting drop [23]. The conditions under which this jet was formed, however, are specific. Pools of liquids such as methanol and acetone produced this phenomenon, while water did not, due to a surface tension higher than that of the drop. At higher impact velocities, the result was separation between the drop and the pool (i.e. cavity formation) [23].

Some researchers have varied the dimensions of the surface to be impacted, using shallow layers of liquids or films [35, 29]. Shin and McMahon observed that droplets ejected vertically after impacts of a liquid drop with a thin liquid layer attain the greatest heights when the depth of the target liquid is equal to the radius of the hemispherical cavity formed by the drop's impact [29]. Yarin focused on the splashes of liquid drops impacting liquid layers thinner than the drop diameter as well as solid surface [35]. In all shallow-pool cases, the main components of the splash are the crown and the droplets that are rebounded upward.

Viscoelastic Fluids

Much attention has been paid to the effect of using a viscoelastic, or slightly non-newtonian, fluid [1, 7, 8, 26, 2, 32]. Cheny and Ogawa both used viscoelastic liquids in their experiments; Cheny used solid spheres impacting the liquid while Ogawa used liquid drops [7, 2]. Both researchers found that the height attained by the Worthington jet was much lower in the case of the viscoelastic polymer solutions

than in that of water, and both attributed this difference to the high viscosity of the liquid[7, 2]. Cheny proposed that the experiment be used as a measure of extensional viscosity because of its simplicity [7]. He later expanded the study by using more solvents as well as multigrade oils, and by using liquid drops in addition to the solid spheres [8].

Following Cheny's claim that the Worthington jet is an extensional flow, and thus a good measure for extensional viscosity, Nigen and Walters looked at the two-dimensional, planar "jet" resulting from the impact of a cylindrical rod with the free surface [26]. Interestingly, they found that the dependence on extensional viscosity is not as great in the planar case as it is in the uniaxial case resulting from impacting spheres; the affect of the addition of the polymer solution was almost unmeasurable [26].

Akers and Belmonte also used viscoelastic fluids impacted by solid spheres, but focused on the motion of the sphere after impact and the cavity formed behind it due to the stretching of the fluid rather than on any upward-ejecting jet [1]. The solution used in their experiments was a "wormlike micellar fluid" [1]. They found that the depth of penetration of the sphere scaled not with Froude number, as in experiments with water as the target liquid, but with the ratio between the initial kinetic energy at impact and the elastic modulus of the liquid [1].

Walters et al. recently examined the effects of viscoelasticity on the Worthington jet, seen experimentally by Cheny, Ogawa and Nigen, by using numerical simulations [32]. His model took into account not only the extensional viscosity of the fluid, but also the normal stress. The results of the simulations agreed with the previous assumptions about the affects of extensional viscosity, but also showed that different physical characteristics (e.g. the viscosity and the stress) of the fluid can oppose each other in determining the behavior of the splash [32].

Granular Jets

Some experimentalists have replaced liquid pools with granular substrates like sand to study impacts of solid objects with a surface [20, 28, 30]. Thoroddsen and Shen

proposed that by studying granular jets ejected after the impact of a solid sphere with sand, it would be possible to isolate the effects of surface tension in similarly-formed liquid Worthington jets [30]. Dimensional analysis was used to determine that the height of the granular jet depends on three parameters: the ratio of the densities of the impacting sphere and the sand, the Reynolds number, and the Froude number [30].

Lohse et al. decreased the size of the granular particles in their experiments and used higher impact velocities to extend their results to large-scale geophysical events [20]. In the cases examined in their study, subsurface pinch off occurs and both an upward and downward granular jet result, just as in the case of hydrophobic-coated spheres impacting water [20]. Because the dynamics of the substrate below the free surface could not be recorded visually, numerical simulations were performed to focus on the cavity evolution and pinch-off [20].

The experiments performed by Royer et al. opposed the theory that granular jets are fully gravity-driven, as in [30, 20]. The results of their high-speed X-ray radiography, which allowed observation of the formation of the jet inside the substrate, led to observation of interaction between the sand and the interstitial air in the medium which defines the formation of the jet [28].

1.1.3 Cavity Dynamics

Richardson developed a potential flow model for the subsurface cavity and measured the resistance on the sphere during impact using the displacement of the sphere with time as recorded using high-speed photography [27]. He also compared the coefficients of drag measured for various types of spheres impacting different liquids and examined the dynamics of spheres hitting the free surface at glancing angles [27].

Mogishi and Squire also focused on the forces on the sphere upon impact, directly measuring the force using a piezoelectric transducer with a hemispherical nose [25]. The data was then used to compare drag coefficients for spheres at different velocities with target liquids of various viscosities [25]. It was found that the dependence of the drag coefficient on Reynolds number on initial impact resembles the dependence for

a sphere moving through homogeneous fluid for a certain range, $0.05 < Re < 5 \times 10^3$ [25].

Gilbarg and Anderson conducted experiments to determine the affect of variations in atmospheric pressure on cavity formation [15]. They found that Froude scaling holds for lower Froude numbers and atmospheric pressures, but that in cases where surface closure occurs, Froude scaling is no longer valid [15]. Their work also briefly mentions the presence of the Worthington jet, but few measurements are able to be made accurately, so the discussion is qualitative [15].

May's experiments varied the air pressure above the surface as well as the shape of the impacting "nose" of the objects, from which he determined that the shape of the nose has no effect on the shape of the cavity formed for cases with equivalent drag forces [24]. All of the cases in the study were cavity-forming due to the high impact velocities used, and so surface closure was also present. Much discussion of the time to surface seal and it's dependence on the density of the air above the water is included [24].

Lee et al. provided a model for cavity dynamics in impact cases where deep pinch-off precedes surface closure, equating the energy transfered into cavity production to the energy dissipated by drag on the impacting body in the fluid [22]. The model was compared to experimental data collected by Gilbarg and Anderson in [15]. The resulting model provides information on the time to deep seal, which is constant, and the location (i.e. depth) of deep seal, which is dependent on the velocity of the impacting body, and thus related to Froude number [22].

Bergmann et al. examined the pinch-off of the cavity resulting from the constant-velocity impact of a cylindrical disk with water for finite Froude numbers, for which cases it was determined that the radius of curvature of the cavity became an important factor [5].

An application of collapsing cavities was studied by Birkhoff in the late 1940's. His work dealt with lining the conical cavity of an explosive with a thin metal layer, so that when the charge is set off behind it, a jet, much like the Worthington jet, is formed with the collapse of the cavity [6]. Using hydrodynamic theory, Birkhoff

characterized both the formation of this high-speed metal jet, and the penetration of the target material by the jet due to the high pressures produced by the impact of the jet with the target surface [6].

Some of the most recent experimental work in spheres impacting the free surface has produced very useful relationships of the time to pinch-off of the cavity and the depth at which pinch-off occurs to Froude number and mass ratio. Yan et al. found through asymptotic analysis and nonlinear numerical simulations, verified experimentally, that for low Froude number cases ($Fr \leq O(10)$) the depth of pinch-off increases linearly with Froude number [17]. Truscott and Techet found that the depth to pinch-off and the depth of the sphere at pinch-off also depends on the mass ratio of the falling sphere, such that for the latter measurement, $d \propto Frm^{*1/2}$, where $Fr = \frac{U_0}{\sqrt{gD}}$ (where U_0 is the velocity of the sphere at impact and D is the diameter of the sphere) and m^* is the ratio of the density of the sphere to the density of water [31]. The non-dimensional time to pinch-off was also found by Truscott and Techet to be proportional to Froude number, where time is non-dimensionalized by impact velocity [31]. This in turn indicates that dimensional time to pinch-off of the cavity is constant when considering single diameters.

1.1.4 Jet Models

Zeff conducted experiments in which an upward jet was produced by Faraday excitation, oscillating the body of water vertically [36]. The collapse of the surface singularity resulting from the excitation and the subsequent jet formed were found to be describable by a single exponent [36].

Some attention has been paid to describing the break up of liquid jets. In 2008, Eggers and Villermaux published a cohesive review of different theories of jet break up, focusing on surface-tension driven effects and including rheological influences [11].

Some recent work on Worthington jet modeling and dynamics has been done by Gekle and Gordillo [14, 13, 16]. Experiments and simulations of a circular disk being drawn vertically into water at a constant velocity were performed, and the formation of the resulting jet was explained in terms of the potential flow of the cavity [14].

A line of sinks is placed at the axis of symmetry of the cavity, and the strength at each depth at pinch-off is then used to describe the formation and behavior of the jet. The jet itself is split into three different regions in Gekle's and Gordillo's work: the acceleration of the fluid from the cavity walls to the jet itself at the base of the jet, the bulk of the jet where velocity is conserved, and the tip of the jet and breakup region [13].

Gordillo and Gekle describe the non-dimensional time to break up and size of droplets ejected at the jet tip by taking into account the strain rate at the base of the jet for each fluid particle that enters the jet and the Weber number, defined as $We = \frac{\rho U^2 R_n}{\sigma}$, where U is the velocity of the fluid as it entered the jet, R_n is the initial radius of the jet, ρ is the density of water and σ is the surface tension. Because it is difficult to measure, and for the purposes of their simulations, R_n is defined as $R_n = 0.5 R_d r_{min}$, where R_d is the radius of the disk and r_{min} is the minimum radius of the cavity before a particle is considered to be in the jet region, which has been numerically determined to be ~ 0.01 [13].

With α defined as the initial value of the non-dimensional strain rate, they define a new dimensionless parameter, We_S, and are able to show that

$$(TS_0) = 2.75 We_S^{2/7}$$

and

$$\hat{r}_{eq} = 0.95 We_S^{-1/7}.$$

Here, $\hat{r}_{eq}$ is the drop radius non-dimensionalized by R_d. The non-dimensional time is measured from the time at which the particle that is at the jet tip at break up enters the jet at the base. These expressions give a simple representation of the time to jet break up and the size of droplets, though the information needed to calculate these values is difficult to measure experimentally [13, 16].

1.1.5 Jet Instabilities and Breakup

An important component of the Worthington jet problem is the breakup of the fluid column. The breakup of a fluid column was quantitatively described by Lord Rayleigh in 1878 [21]. Today, the Rayleigh-Plateau instability is commonly used to describe droplet formation from perturbations in the fluid column, where the dispersion relationship between the growth rate and wavelength of the perturbation is well known. In the context of Worthington jets, Rayleigh-Plateau can provide insight into the parameters that trigger breakup, which corresponds to height and velocity information inherent in the jet. The parameters of the Worthington jet problem are altered from the canonical Rayleigh-Plateau situation, but the theory provided by Rayleigh serves as a good starting point for further analysis of the breakup and overall behavior of Worthington jets. In this thesis, the breakup of Worthington jets formed after hydrophobic sphere impacts will be compared to standard Rayleigh-Plateau dissolution into droplets so that further insights into the fluid dynamics can be obtained.

The goal of this thesis is to determine experimentally some simple scaling laws of Worthington jet characteristics with readily obtained non-dimensional parameters, and to gain some physical insight into the overall behavior of these jets under varying initial conditions.

1.2 Outline of Thesis

In Chapter Two, the experimental methods used to acquire the data discussed in this study are described. Relevant experimental parameters are defined and the test matrix outlined. The apparatus is described and some of the image processing detailed.

Chapter Three introduces unprocessed results of the experiments, including qualitative discussions of some of the cases. Select images that form a broad representation of the entire study are shown. Time series sequences of images are used to compare results across mass ratio and Froude number. Single images of maximum height events are also shown and compared.

Chapter Four is a discussion of the results for both hydrophobic and hydrophilic

spheres. A full set of relevant dimensionless parameters is defined, and dependence of the Worthington jet characteristics on these parameters is given. Experimental error is determined and inconsistencies in the results discussed. Rayleigh-Plateau instabilities are introduced and discussed in relation to the measured characteristics of the Worthington jets formed in hydrophobic cases.

Conclusions of this study and directions for future work are presented in Chapter Five.

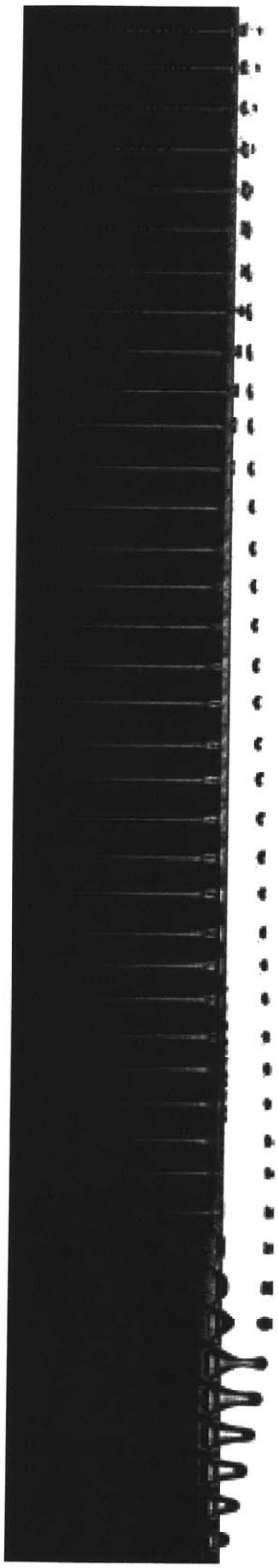

Figure 1-1: A Worthington jet erupts from the cavity created by a $1in$ diameter acrylic sphere impacting the free surface. Initial height of the sphere above the water is $30cm$.

Chapter 2

Experimental Methods

Experiments were conducted to gather information about the Worthington jets formed when both hydrophilic and hydrophobic solid spheres of diameter 1 inch are dropped from various heights above the free surface. Height and temporal data were collected, and general observations about the images were recorded.

2.1 Apparatus

The experiments were conducted using a rimless glass aquarium, $18 \times 18 \times 24$ inches in size. The tank was filled to the brim and was sitting on the floor with a shallow pan under it to catch overflowing water. Spheres were placed in a camera aperture fixed to a horizontally translating arm, and were released from rest manually. The camera aperture ensured that the spheres had minimal angular and horizontal velocities as they hit the free surface. The frame on which the aperture and arm were mounted was composed of 80/20, and the arm contained two sections connected by a slider for retraction. Once a sphere was released, the arm could be quickly slid out of the field of view of the camera and out of the path of the Worthington jet.

Images were acquired using an IDT Motion Pro X3 camera with a 24mm Nikor lens. The frame rate was set to 500 frames per second. The field of view of each image includes both above and below the free surface, which are captured simultaneously from the single camera. Example images are shown in Figure 2-2. A single bank of

fluorescent lights behind the tank was used to accomplish proper lighting. A thin strip of black backing, the width of the field of view of the images, was placed above the waterline in front of the light bank. Below the free surface, a white diffuser was placed in front of the light bank. This configuration was found to give the best results for clear visualization of activity both above and below the free surface. A simple representation of the setup is shown in Figure 2-1.

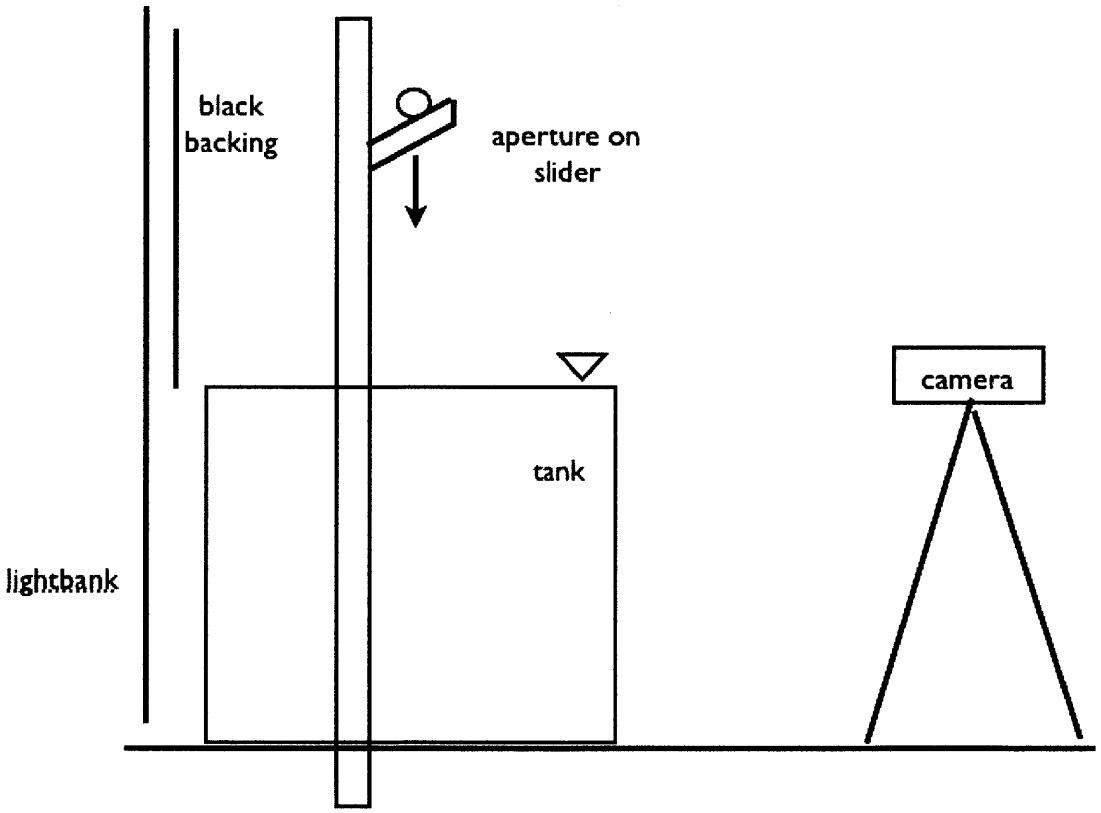

Figure 2-1: Experimental set up.

2.2 Test parameters

All spheres used were of a diameter of 1 in., or 0.0254 cm. Three different materials were used to vary mass ratio compared to water: acrylic, ceramic, and steel. The mass ratios, (i.e. the density of the material compared to that of water), m^*, of the three materials are given in Table 2.1.

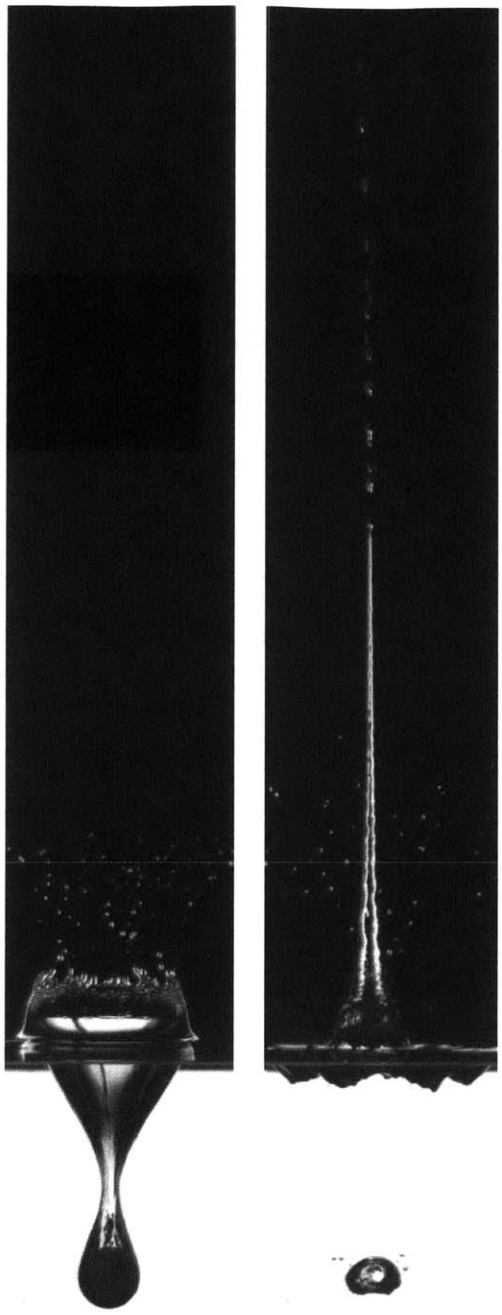

(a) Image with sub-surface detail

(b) Image with above-surface detail

Figure 2-2: The two images above demonstrate the field of view captured by the camera. The cavity and other sub-surface features are clearly visible, as are the splash and jet above the surface.

Hydrophobicity is measured by the wetting angle of water on a surface, θ. Values of θ greater than 90^o indicate hydrophobic surfaces, while surfaces with a wetting angle

Table 2.1: Mass ratios of the materials used

Material	Mass Ratio
Acrylic	1.2
Ceramic	3.9
Steel	7.8

less than 90^o are considered hydrophilic. In this experiment, half of the spheres were coated with Cytonix Corporation WX2100 weatherproofing spray, resulting in $\theta \geq 100^o$. The other spheres were made hydrophilic, with $\theta \leq 70^o$, by being thoroughly cleaned using a sequence of solvents. In a chemical hood, these spheres were wiped clean first with acetone, followed by isopropyl alcohol, and finally ethanol. Time was allowed between application of each chemical for drying. Clean spheres were handled only with latex powder-free gloves and were kept in clean, closed containers to prevent dust from settling on them.

A sphere of each material and surface treatment was released from 10 different heights above the free surface resulting in 10 impacting Froude numbers, defined as

$$Fr = \frac{U_0}{\sqrt{gD}}$$

, where U_0 is the velocity of the sphere at impact, D is the diameter of the sphere, and g is the gravitational constant. Heights used and their corresponding Froude numbers are shown in Table 2.2.

Due to the restrictions of the 80/20 structure supporting the arm with the aperture, there was a gap between drop heights of 7 cm and 24 cm. However, for the purposes of this study, a wide enough range of Froude numbers was observed to produce reasonable results.

Between cases, the water in the test tank was allowed to settle so that no residual dynamics altered the results of the next drop. It was found that the hydrophobic coating wore off of the spheres with each drop, especially from the impact of the spheres with the floor of the tank. As a result, the coating came off very unevenly, affecting the consistency of the hydrophobic results. Hydrophobic spheres were thus

Table 2.2: Heights and corresponding Froude values.

Height [cm]	Froude number [N/A]
7	2.35
24	4.35
30	4.86
36	5.32
42	5.75
48	6.15
54	6.52
60	6.87
66	7.21
72	7.53

recoated after three runs to try to ensure uniform surface properties. Cases were repeated as needed to obtain confident results. The jets produced can very greatly due to the slightest variation in sphere coating, any horizontal velocity on impact, or any rotation induced by the release mechanism.

To determine an estimate of the experimental error encountered in the trials, two hydrophobic cases were repeated ten times. Acrylic and ceramic hydrophobic spheres were dropped from 30 cm ($Fr = 4.35$) and the images compared. Hydrophilic cases were not repeated to such an extent because the results were much more uniform for those cases.

2.3 Data Processing

2.3.1 Calibration

All data were gathered directly from the images obtained. To ensure that the heights measured were reliable, proper calibration of the images was important. A checkerboard grid of 1 inch squares was used to determine any vertical or horizontal distortion of the images. Upon inspection in Matlab®, the variation in scale throughout the field of view was negligible. For each trial, a calibration constant was found by finding the boundary of the sphere in Matlab®, which is given in pixels, and determining

the diameter from that information. This figure was then divided by the known diameter of the sphere to give the constant in $\frac{pixels}{meter}$. Due to diffraction, the calibration constant below the free surface was found to be different than that above the free surface. This becomes important when information about the depth and velocity of the sphere after impact is measured.

2.3.2 Height Measurements

Matlab® was used to create custom scripts for extracting information from the raw images. One of these scripts was developed to find the height of the Worthington jet for every step in time. The height measured was that of the continuous jet, so as droplets break away from the jet tip, they are no longer accounted for in the height measurement. Once fluid droplets separate from the tip of the Worthington jet, or when the jet breaks down to form a stream of droplets, those fluid parcels are no longer tracked, so their velocity and height information are lost. The measurement of only the continuous fluid column leads to sudden, large decreases in measured jet height, as seen in the case of an acrylic hydrophobic sphere dropped from a height of 30 cm, shown in Figure 2-3. The decrease in height measured at 0.333 seconds in the figure coincides with the breakdown of the jet into droplets. The jagged peaks in the measurement when the jet is at its greatest height coincide with the release of droplets from the jet tip as it moves upward.

The majority of the information used for further analysis of the Worthington jet comes from this height measurement. The error in this measurement stems from the resolution of the images, with each measurement accurate to within one pixel. The error on each height found is then $\pm 0.06cm$, based on the calibration constant. From this data, jet tip velocity can be calculated and used to characterize the formation of the jet.

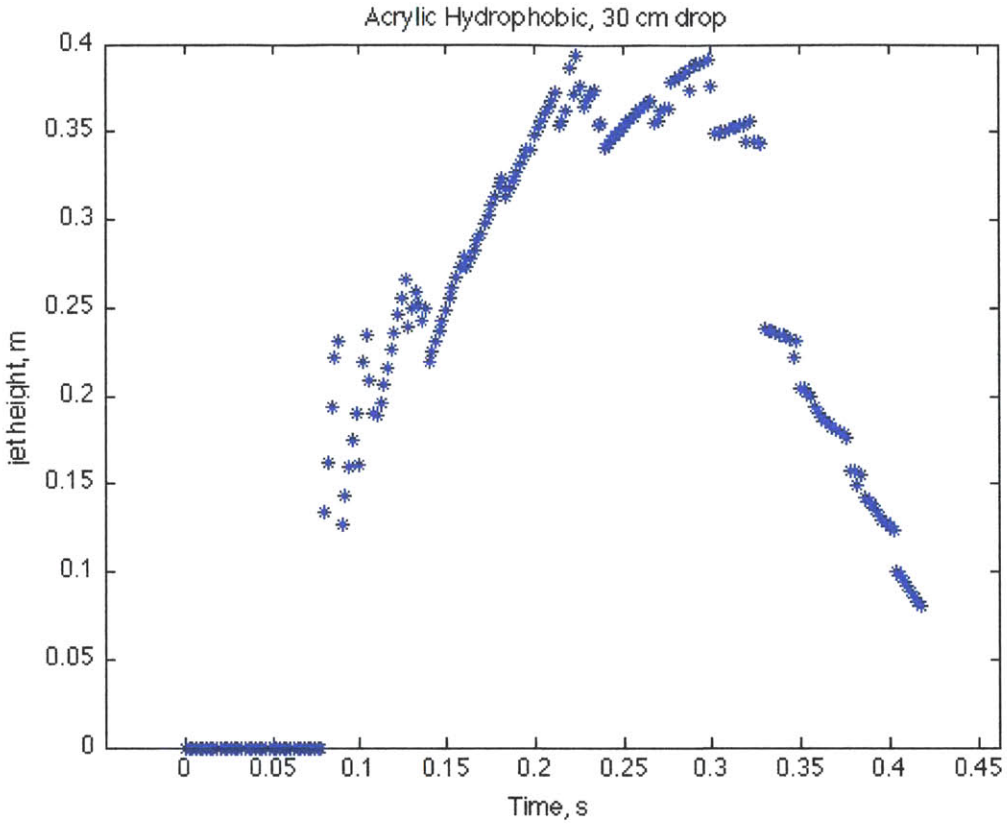

Figure 2-3: Height of the continuous jet as it evolves with time for a hydrophobic acrylic sphere dropped from 30 cm (Fr = 4.86).

2.3.3 Cavity Measurements

The other piece of information that is helpful in explaining the behavior of the Worthington jet in hydrophobic cases is the evolution of the cavity. The position and velocity of the cavity walls can be used to define potential flow around pinch-off, which can then be used to determine characteristics of the Worthington jet, but in this study, the most important information from the cavity is the time and depth of pinch-off.

Chapter 3

Results

3.1 Hydrophilic Cases

In this section, images from the hydrophilic set of experiments are shown. A wide range of the results are listed here, but images for every case are not presented in detail. The cases represented demonstrate the most important features and characteristics to be discussed, giving an overview of the complete results of the study. Data from the full set of cases will be presented cohesively in Chapter Four.

3.1.1 Two Regimes of Jet Formation

One characteristic of Worthington jet formation in the hydrophilic cases, which will be used for organizing further observations of these cases, is the occurrence of two separate jets upon impact of the sphere. These regimes will simply be denoted by the "first" and "second" jets, respectively, based on the temporal separation between the two.

Figure 3-1 shows the impact of a hydrophilic sphere resulting in a Worthington jet. In this case, an acrylic sphere fell from a distance of 24 cm above the free surface, impacting with a Froude value of $Fr = 4.35$. Every frame in the sequence is shown here, so images are separated by 2 ms in time. In the fourth frame, the thin film of fluid splashing up and around the sphere is visible, and is seen to meet at the top of

the sphere 4 ms later in the sixth frame. This fluid is then forced upward into a thin, fast-moving jet. Note that the top of the sphere is still above the level of the free surface as this happens. This is the first regime of the Worthington jet. The first, thin jet continues to form until the ninth frame, when the sphere is fully submerged. Due to the diffraction in the images at the air-water interface, the sphere does not appear to be completely submerged in the ninth frame. The diffraction is a result of the camera not being at a height parallel to the free surface (the camera was angled slightly downward). Though some of the detail just below the free surface is lost, the entire jet is visible. The angling of the camera is small enough that it is assumed not to affect the measurements of height taken from the free surface.

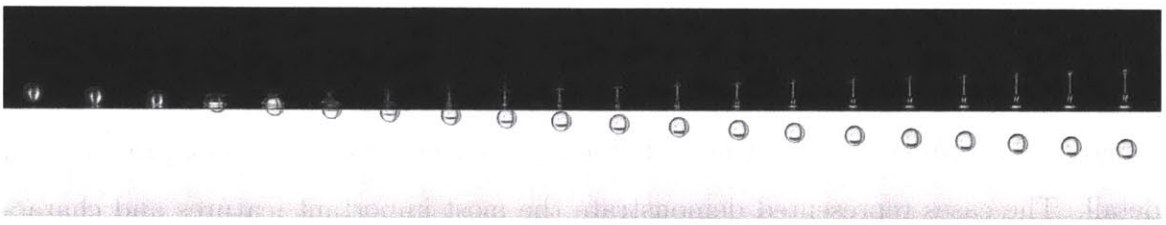

Figure 3-1: The initial impact of a hydrophilic acrylic sphere with drop height of 24 cm ($Fr = 4.35$) is shown. Two stages of the jet are seen. The faster, thinner jet is formed when the sphere has not yet been fully submerged, and the slower, broader jet follows once the sphere is completely below the free surface.

After the formation of the first jet and the complete submersion of the sphere, the second jet is ejected. This jet is broader than the first, and is seen first in the tenth frame of Figure 3-1. The second jet is comprised of the fluid displaced by the sphere after it is fully submerged. It has a speed less than that of the first. An important result of this double jet is the occurrence of two separate breakup events. The first jet, which is the faster of the two, breaks into droplets much earlier than the second jet. This second jet will often only eject one droplet before falling back into the fluid.

The designations of first and second jet will be used in the following sections to distinguish between observations of the two independent developments, as each jet has separate measured characteristics.

3.1.2 Froude Number and Mass Ratio Comparisons

Two groups of sequences can be used to compare the effects of Froude number and mass ratio on the development of both the first and second Worthington jets. Figure 3-2 compares three spheres falling at the same impacting Fr, with different masses. Each sphere fell from 36 cm, so that on impact $Fr = 5.32$. Images in the sequence are separated by 4 ms. The two separate jets become more apparent in these images, with the first jet breaking quickly into droplets that continue moving upward while the second remains continuous nearer the surface. In the acrylic case shown in Figure 3-2(a), one droplet is ejected from the tip of the second jet in the 25th frame, earlier than in the steel case in Figure 3-2(c), where the droplet is ejected in the 30th frame. In the ceramic case, a droplet fails to form in the second jet. The tip of this jet is seen to tend to the right. This is a result of some imperfection in the experiment. Either the surface of the sphere was not perfectly clean or, less likely, there was some horizontal component to the sphere's velocity on impact.

Imperfections in the experiment such as those demonstrated in Figure 3-2(b) are unfortunately common. This makes interpretation of the results difficult and increases the error in measurements. However, conclusions presented in this study take these imperfections into account.

Returning to the comparison of the cases in Figure 3-2, we see that the maximum height reached by the second jet increases with increasing mass ratio. The maximum height attained by the first jet, however, does not seem to follow the same trend. At this Fr, the acrylic sphere produces the highest first jet, followed by the steel and ceramic cases, respectively. The experimental error in the ceramic case (evident from the tendency of the tip of the second jet to the right) can be expected to greatly affect the evolution of the first jet. However, upon inspection of all of the images gathered for all values of Fr, the maximum heights of this first jet do not tend to follow any sort of trend with respect to mass ratio.

The next cases examined are those of an acrylic sphere with three different values of Fr. Figure 3-3(a) is the same case as in Figure 3-2(a), with $Fr = 5.32$. Figure

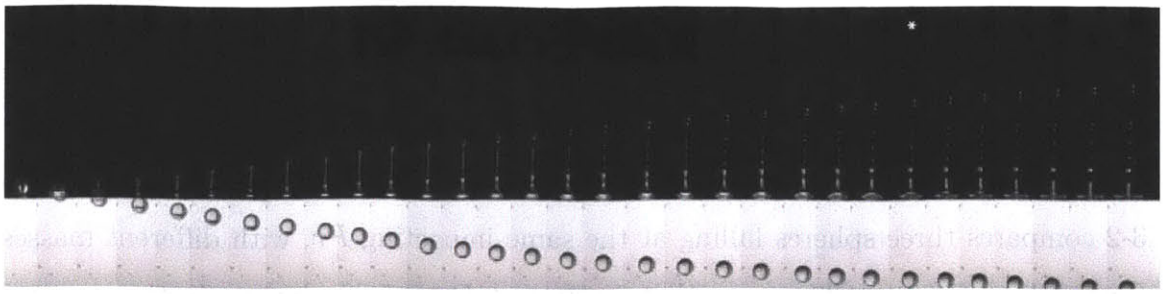

(a) Acrylic hydrophilic sphere, 36 cm

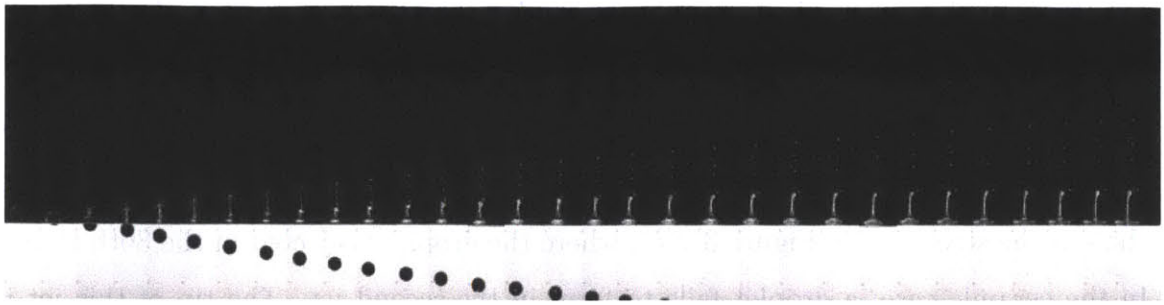

(b) Ceramic hydrophilic sphere, 36 cm

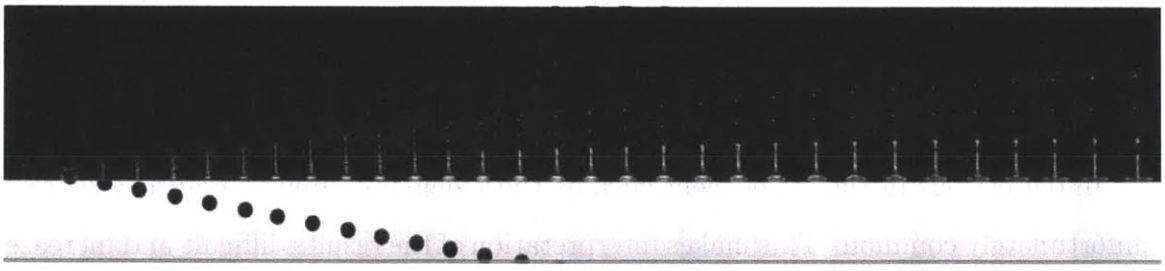

(c) Steel hydrophilic sphere, 36 cm

Figure 3-2: Figures (a) through (c) show hydrophilic spheres impacting the free surface from height of 36 cm ($Fr = 5.32$). Every other frame is shown, giving a separation of 4 milliseconds between each image in the sequence.

3-3(b) is an acrylic sphere with $Fr = 5.75$, and Figure 3-3(c) shows an acrylic sphere with $Fr = 6.87$. Images in each of the three sequences are separated by 4 ms.

Between the three sequences in Figure 3-3, we can see that both the first and second jets are formed at the same time regardless of Fr. It is also apparent that the maximum height of the second jet increases with increasing Fr, which is expected as increasing impact velocities would seem to result in faster jet velocities. The first jet is not as predictable; the $Fr = 5.32$ case produces the highest maximum height with the two larger Fr cases producing heights very similar to each other. The time at which each jet breaks up is another characteristic of interest, and is shown to decrease

with increasing Froude number. The first jet starts to break up in the 13th frame of the lowest Fr case, in the 10th frame of the middle case, and in the 7th frame of the highest Fr case. The first jet in Figure 3-3(c) is very messy, however. This is assumed to be a result of the higher impact velocity. The first jet, because it forms before the sphere is fully submerged, is most likely limited by the wetting ability of the fluid. There may also be surface imperfections on the sphere in this case, as implied by the rightward tendencies of the spray from the first jet. In contrast, the breakup of the second jet appears to be independent Fr, occurring near the 25th frame in all three cases.

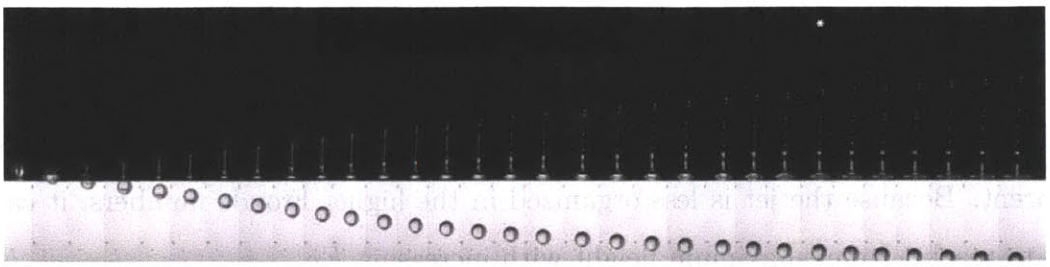

(a) Acrylic hydrophilic, 36 cm

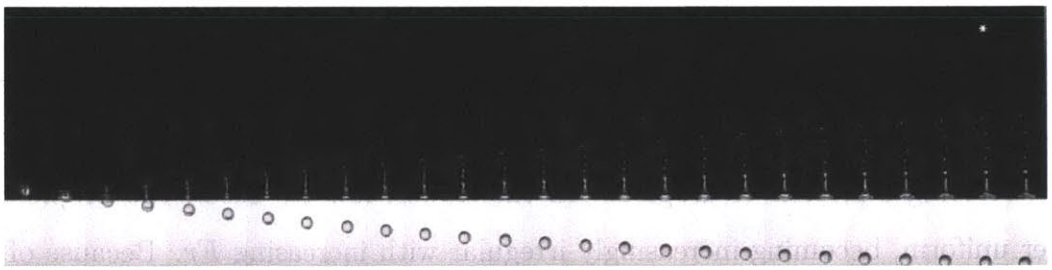

(b) Acrylic hydrophilic, 42 cm

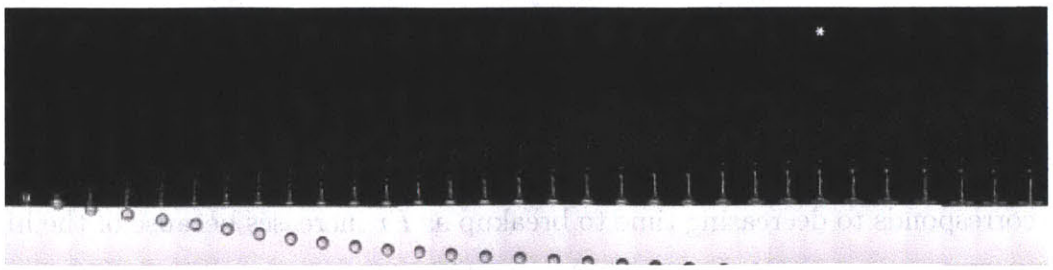

(c) Acrylic hydrophilic, 60 cm

Figure 3-3: Figure (a) shows the evolution of the Worthington jet for an acrylic hydrophilic sphere with $Fr = 5.32$ on impact. Figure (b) shows the same sphere impacting with $Fr = 5.75$, and the final sequence shows the $Fr = 6.87$ case. The 25th frame in each sequence is marked by an asterisk, and the time between images is 4 milliseconds.

The First Jet

To better examine the processes of the first jet and how it compares across mass ratio and Froude number, it is useful to compare images of the maximum heights of the jet for each case. Figure 3-4 accomplishes this. We see the maximum heights of the first, thin jet. The $Fr = 2.35$ case is not included in these sequences because the first jet is not present with that low of an impact velocity. Across all three mass ratios, it is clear that there is no apparent trend in the maximum heights of this first jet. Those in the lower Froude number cases are much cleaner than those formed in the higher Fr cases. This is expected due to the higher energy transfered into the thin film that covers the sphere when the impact speed is greater. Instabilities in the high Froude number cases are much more likely, and the subsequent affect on the jet is apparent. Because the jet is less organized in the higher Froude numbers, it can be seen to reach a lower maximum height with increasing Fr.

Another interesting characteristic to note in Figure 3-4 is the time at which the breakup in each of these cases occurs. The images chosen occur one to two frames before breakup of this first jet. In most cases, the entire jet breaks up simultaneously, forming a stream of droplets. In the slower, low Fr cases, the droplets are rather uniform, becoming increasingly irregular with increasing Fr. Because of this characteristic of the breakup of the first jet, the maximum height of the continuous fluid jet, which is the primary measure throughout this study, occurs just before the breakup event. The depth at which the sphere is seen in the images in Figure 3-4 appears to be approximately at the same depth for all Froude numbers ($\pm 1 diameter$). This corresponds to decreasing time to breakup as Fr increases because of the higher sphere velocities beneath the free surface with increasing Fr. It also appears that the time to breakup is independent of mass ratio, which would suggest that the first jet is a direct result of the initial impact, having no dependence on the deceleration of the sphere once it enters the fluid. The decrease with increasing Froude number most likely corresponds to the speed with which that first fluid film travels around the sphere, which is proportional to the speed of impact.

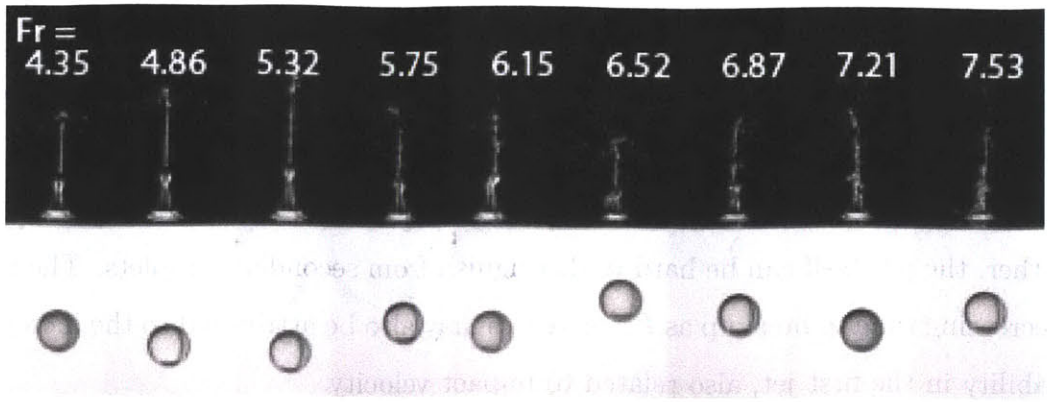

(a) Acrylic maximum 1st jets for each Fr

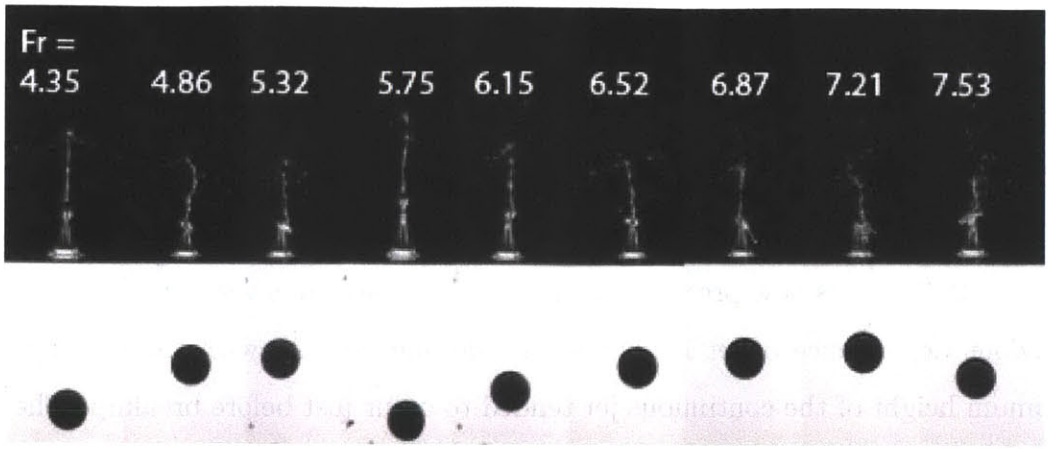

(b) Ceramic maximum 1st jets for each Fr

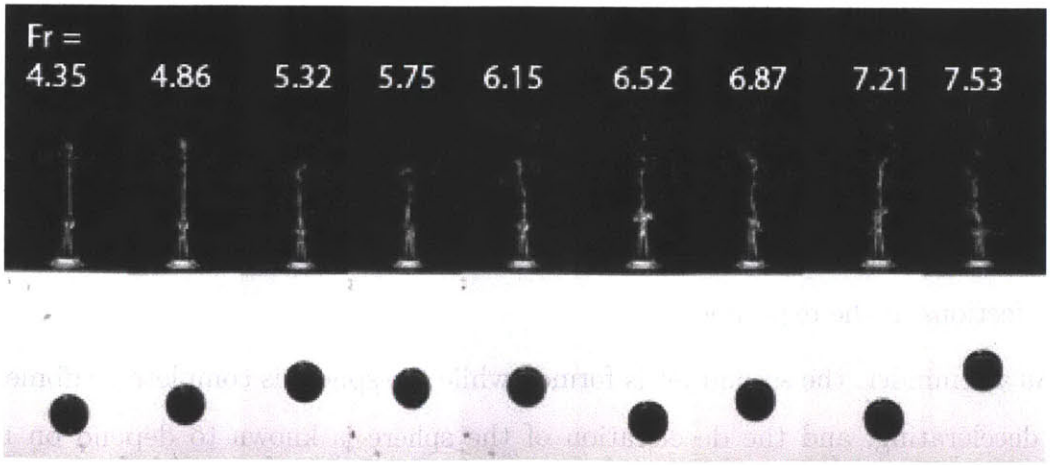

(c) Steel maximum 1st jets for each Fr

Figure 3-4: First jets at maximum height are shown for each Fr, with $Fr = 4.35$ on the far left, increasing to $Fr = 7.53$ on the far right. Maximum height is assumed to occur just before breakup of the jet.

Analysis of the images to determine time to breakup was difficult, as it was challenging to find precisely where breakup of the first jet occurs in cases where its formation is messy, such as those with high Fr. If there is a lot of spray outside of the first jet, occurring typically at the top of the sphere as the thin fluid layer comes together, the jet itself can be hard to distinguish from secondary droplets. The trend of decreasing time to breakup as Fr increases may also be attributed to the increasing instability in the first jet, also related to impact velocity.

The Second Jet

Figure 3-5 compares the maximum heights of the second jet for the hydrophilic cases for the purpose of comparing both Froude number and mass ratio effects. Note that the $Fr = 2.35$ case is now present, though the "jet" formed is very small. Here, there is obvious dependence of jet height on Froude number. As with the first jets, the maximum height of the continuous jet tended to occur just before breakup. The only exceptions to this occur in the lower Fr cases, where a droplet may not be ejected from the jet until it has almost fallen back into the fluid. It is difficult to see in the images any dependence of maximum height on the mass ratio. Looking at Figure 3-5, errors and variations in the experiment are evident from jets that are tending to one side or from droplets that are seen forming asymmetrically or irregularly. The linear trend in maximum height is still evident, however, despite the added error from imperfections in the experiment.

As a reminder, the second jet is formed while the sphere is completely submerged and decelerating, and the deceleration of the sphere is known to depend on mass ratio, with spheres of lower mass decelerating more rapidly. If the second jet is comprised mainly of fluid displaced by the sphere once it is submerged, a sphere that is moving more quickly under the free surface, displacing more fluid per unit time, can be expected to form a higher jet. Time to breakup of the second jet appears to have little predictability or correspondence to either Froude number or mass ratio. It is almost constant, but with much variation.

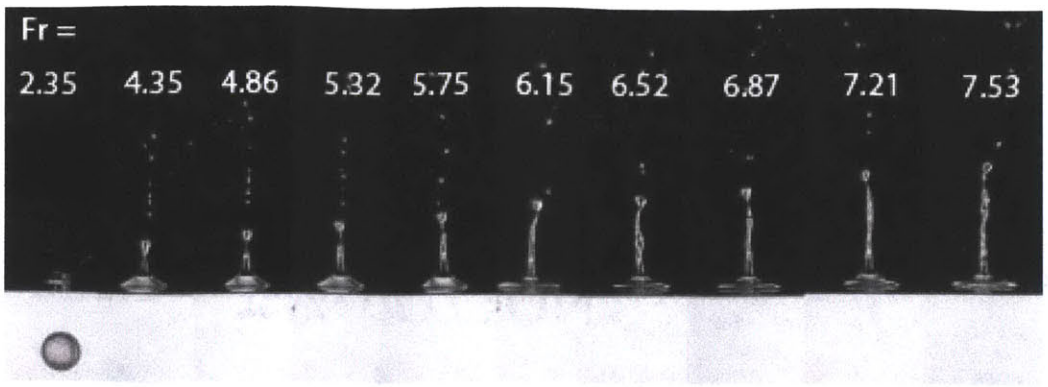

(a) Acrylic maximum 2nd jets for each Fr

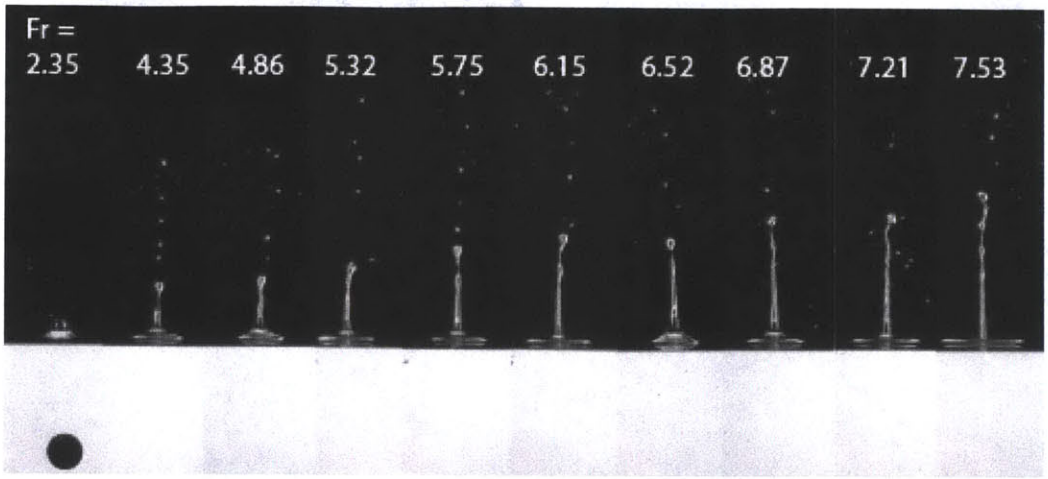

(b) Ceramic maximum 2nd jets for each Fr

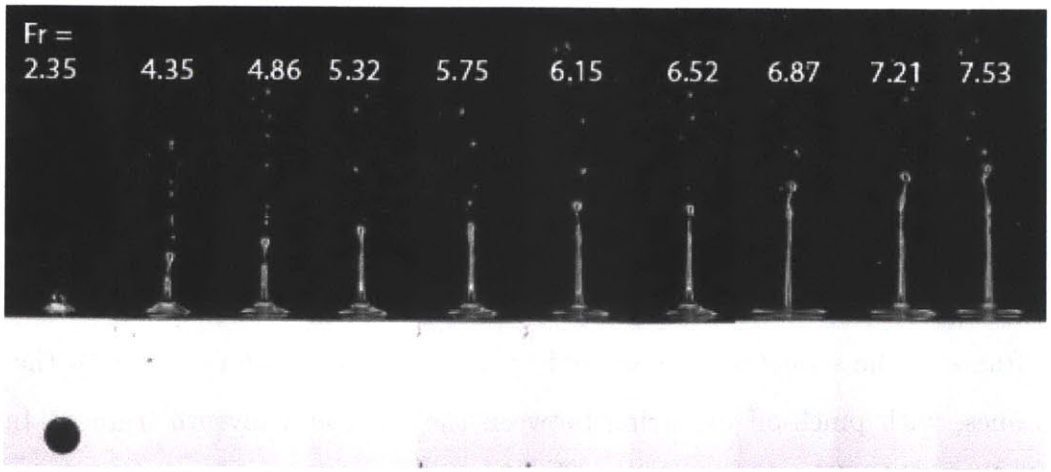

(c) Steel maximum 2nd jets for each Fr

Figure 3-5: Second jets of maximum height are shown for each Fr, with $Fr = 2.35$ on the far left, increasing to $Fr = 7.53$ on the far right. The time between images is 4 milliseconds.

3.2 Hydrophobic Cases

This section features results from the hydrophobic set of experiments. Representative sequences have been chosen to produce a complete picture of the results obtained.

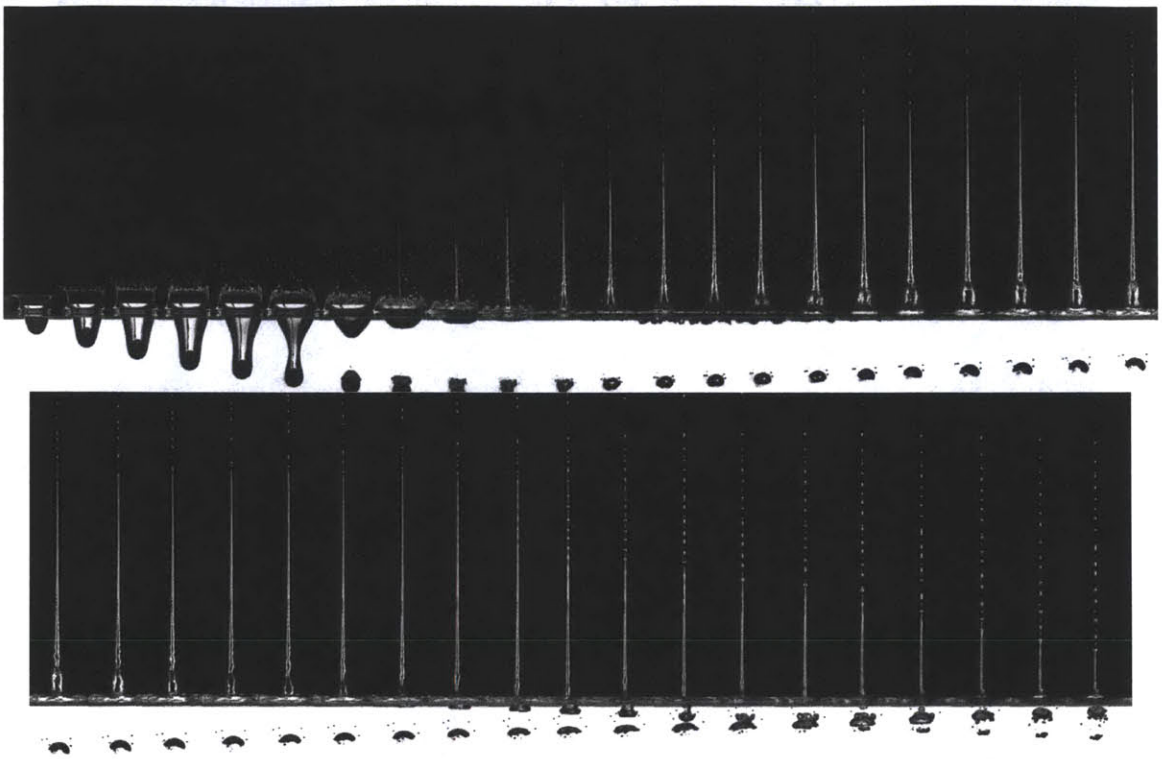

Figure 3-6: Evolution of the Worthington jet formed by a hydrophobic acrylic sphere dropped from a height of 30 cm ($Fr = 4.86$). Images shown are separated by 10 milliseconds.

Figure 3-6 is one example of a typical hydrophobic case. The acrylic sphere was dropped from an initial height of 30 cm, giving it an impacting Froude value of 4.86. Each frame in the sequence is separated by 10 ms. The cavity is visible in the first six frames, with pinch-off occurring between the sixth and seventh frames. In the eighth frame, the Worthington jet is finally visible, and already at a great height above the free surface. The droplets that make up the spray at the very tip of the jet soon travel outside the field of view. The continuous jet proceeds to travel vertically until individual droplets begin breaking off at an average maximum height. Finally, in frame 30, instabilities in the bulk of the jet are seen to start forming droplets, and two frames later over half of the column is broken up. At this point, the jet and all

ejected droplets are falling back to the free surface.

An interesting characteristic to note in this and subsequent image sequences is the air bubble that remained attached to the sphere after pinch-off. It eventually breaks off of the sphere and we see it rising back to the surface from the tenth frame onward.

As has been shown in previous work, the time to pinch off of the cavity in hydrophobic sphere impact experiments is equal for all Froude values, while the depth at which it occurs is dependent on Fr. In Figure 3-7, the cavities formed by two different values of Fr for an acrylic hydrophobic sphere are shown. In Figure 3-7(a), the sphere has an impacting Froude number of 4.35, while the sphere in Figure 3-7(b) has a value of $Fr = 5.75$. Images in both sequences are separated by 10 ms. The cavity for the $Fr = 5.75$ case is elongated when compared to the $Fr = 4.35$ case and pinch off happens at a deeper depth, but the time at which it occurs is between the tenth and eleventh frame in both sequences, so just greater than 90 ms. The exact moment of pinch off is not shown in these sequences, but is compared in Figure 3-8. Here, it is very clear that the depth of pinch off is affected by the impacting Froude number, as it is expected to be. In this pair of images, the difference in the splash crown is also evident. The lower Fr value splash has much less energy, and is seen to have already begun breaking up at pinchoff. The top of the splash in the $Fr = 5.75$ case is out of frame, but the curvature towards the center of the impact site is evident.

3.2.1 Surface Closure

A result of hydrophobic cases that is not encountered in the hydrophilic cases in this study is the occurrence of surface closure. Figure 3-9 shows a case of a sphere impacting the free surface with a Fr value high enough to cause closure of the surface splash. This surface closure occurs before the time of pinch off of the cavity. The sphere is steel, and the impacting Froude number is 5.32. This corresponds to a drop height of only 36 cm, however the high mass ratio of the steel affects the occurrence of surface closure prior to pinch off. It was found that surface closure occurs with acrylic spheres that have $Fr > 6.34$, with ceramic spheres that have $Fr > 5.47$, and with steel spheres that have $Fr > 4.86$.

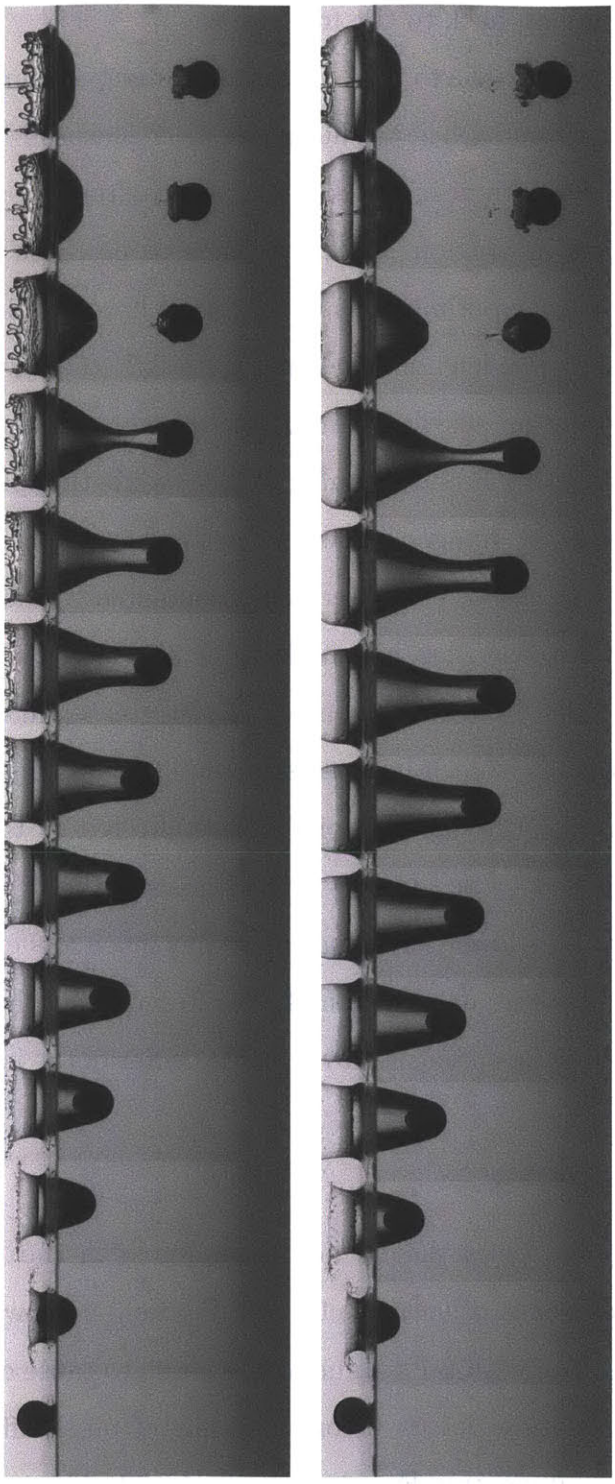

(a) Acrylic hydrophobic cavity, 24 cm

(b) Acrylic hydrophobic cavity, 42 cm

Figure 3-7: Cavities formed by the impact of acrylic hydrophobic spheres are shown. $Fr = 4.35$ in (a) and $Fr = 5.75$ in (b). The time between images is 10 milliseconds.

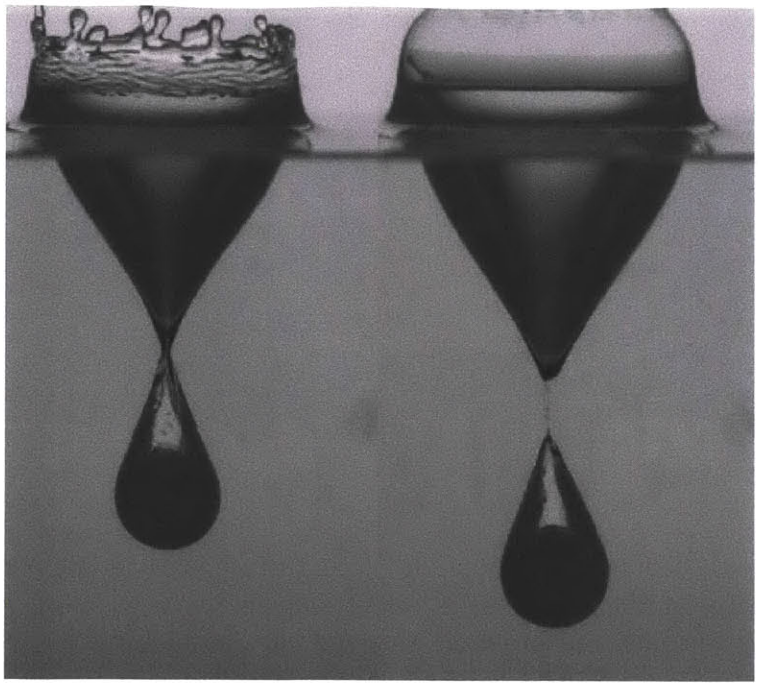

Figure 3-8: The moment of pinch off for the $Fr = 4.35$ and $Fr = 5.75$ cases are shown for a hydrophilic acrylic sphere.

In the example of surface closure in Figure 3-9, the affect of the closure on the formation of the Worthington jet is apparent. Spray is emitted when surface closure occurs, and when the jet erupts from the location of pinch off, it must break through the closed bell on the surface. The jet is seen to break through, but it is much altered, and does not travel nearly as high, having been hindered by the closed surface. Droplets still manage to reach impressive heights, again traveling out of the field of view, but the continuous jet is much smaller and less organized than in cases without surface closure.

The next group of image sequences compares three cases with different mass ratios, all at $Fr = 7.53$, so that surface closure occurs in all three cases. Time between the images in Figure 3-10 is 20 ms. The main feature we see in these sequences is that as mass ratio increases, the closed dome collapses towards the free surface more before the Worthington jet is formed and attempts to break through. The result is that the acrylic case shown in Figure 3-10(a) has the most pronounced jet-type structure, and the steel case in Figure 3-10(c) has the least defined structure of the three. It was

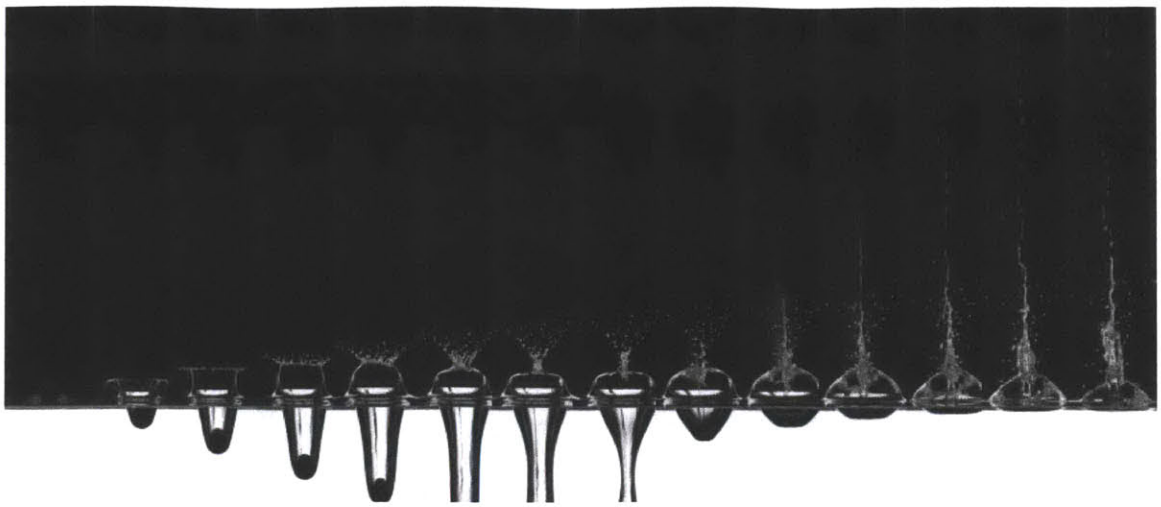

Figure 3-9: A steel sphere impacts the free surface with a high enough velocity for surface closure of the cavity to precede deep seal ($Fr = 5.32$), resulting in the Worthington jet striking and breaking through the closed dome.

observed during the experiments that cases with surface closure were accompanied by a loud plopping sound, which occurred as the fluid erupted through the dome.

These cases which involved surface closure were not measurable in terms of the features of the Worthington jets which this study aims to characterize. However, there are still many interesting observations to be made in the very high Froude number cases.

3.2.2 Froude Number and Mass Ratio Comparisons

The next set of figures compare different hydrophobic cases with each other to distinguish differences caused by varying Froude number and mass ratio, just as with the hydrophilic cases previously. The first comparison is of the three mass ratios with Fr held constant. Figures 3-11(a), 3-11(b), and 3-11(c) show an acrylic, ceramic, and steel sphere, respectively, falling from a height of 24 cm. At this Froude value of 4.35 on impact, none of the cases have surface closure. Images in the sequences are 20 ms apart.

The ceramic case has some error, evident through the leaning of the Worthington jet as it first appears in frame five. The jet appears to straighten under its own

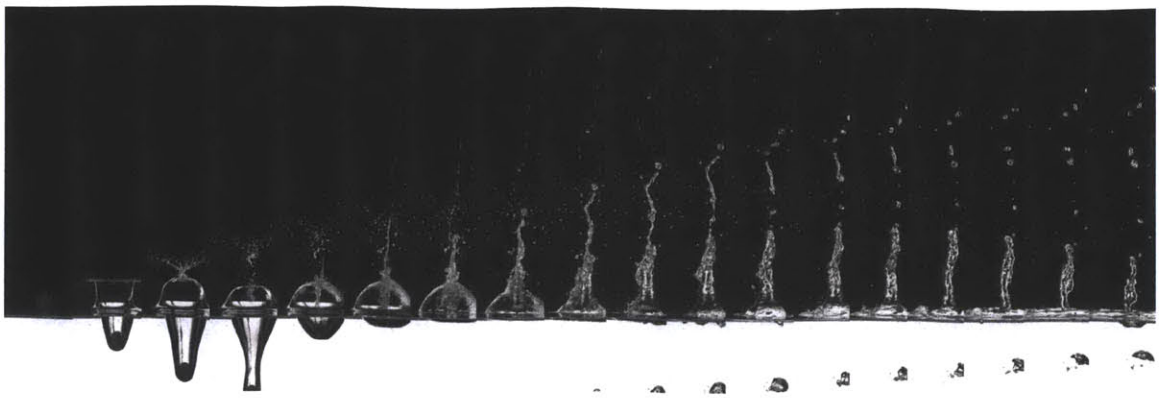

(a) Acrylic hydrophobic jet, 72 cm

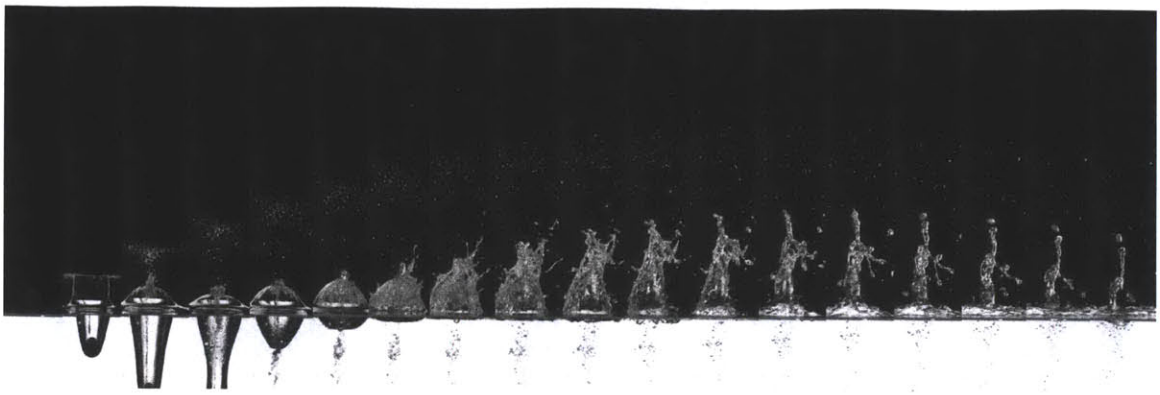

(b) Ceramic hydrophobic jet, 72 cm

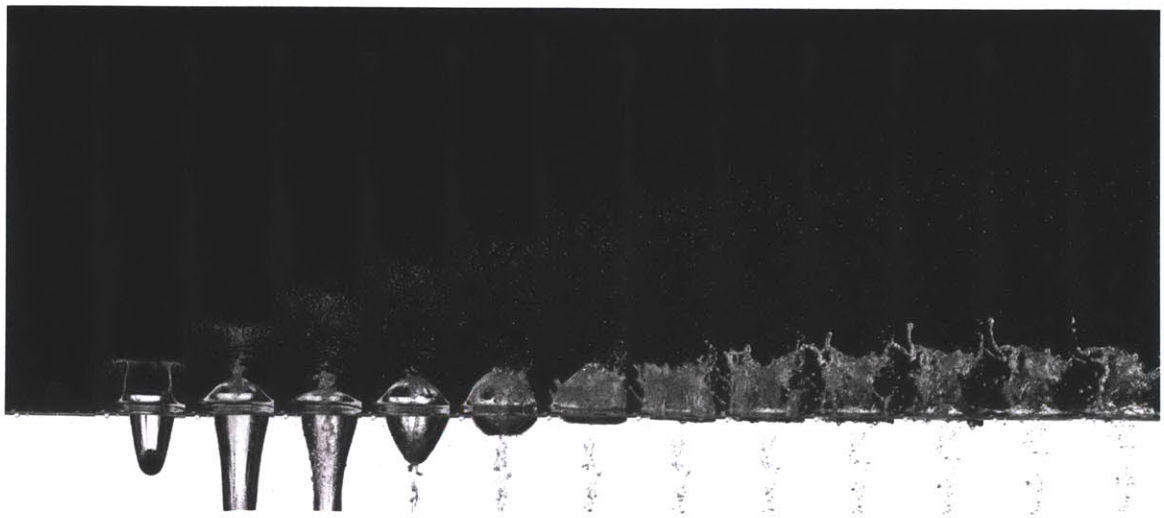

(c) Steel hydrophobic jet, 72 cm

Figure 3-10: Jets formed from impact of hydrophobic spheres with $Fr = 7.53$ are shown. Acrylic, ceramic, and steel spheres are used, and surface closure precedes deep seal and Worthington jet formation in all three cases. The time between images is 20 milliseconds.

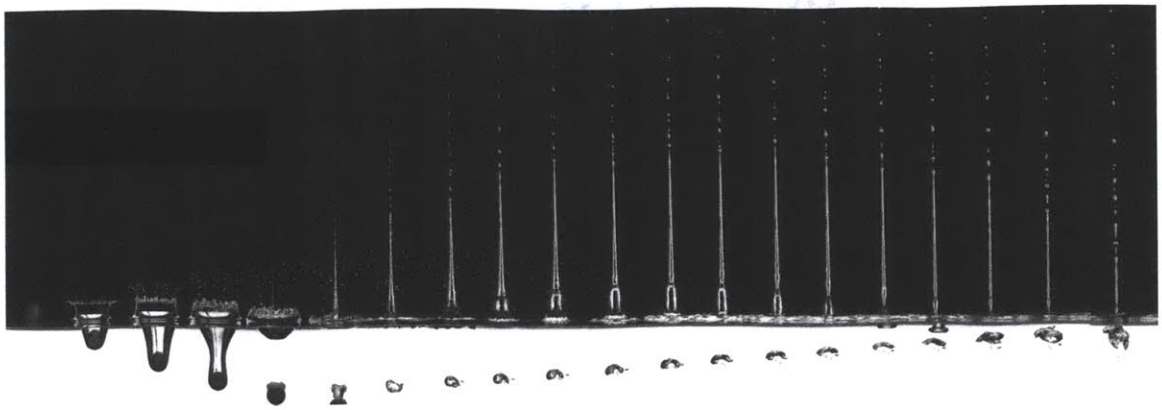

(a) Acrylic hydrophobic jet, 24 cm

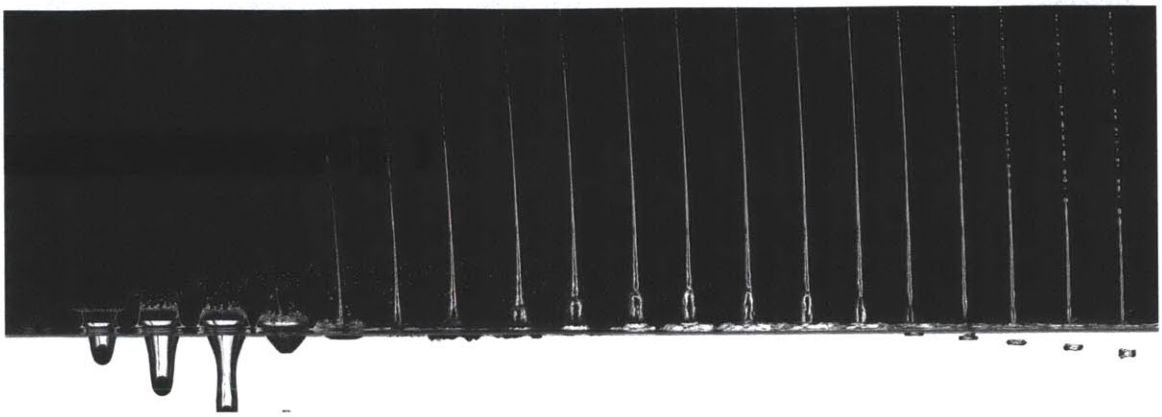

(b) Ceramic hydrophobic jet, 24 cm

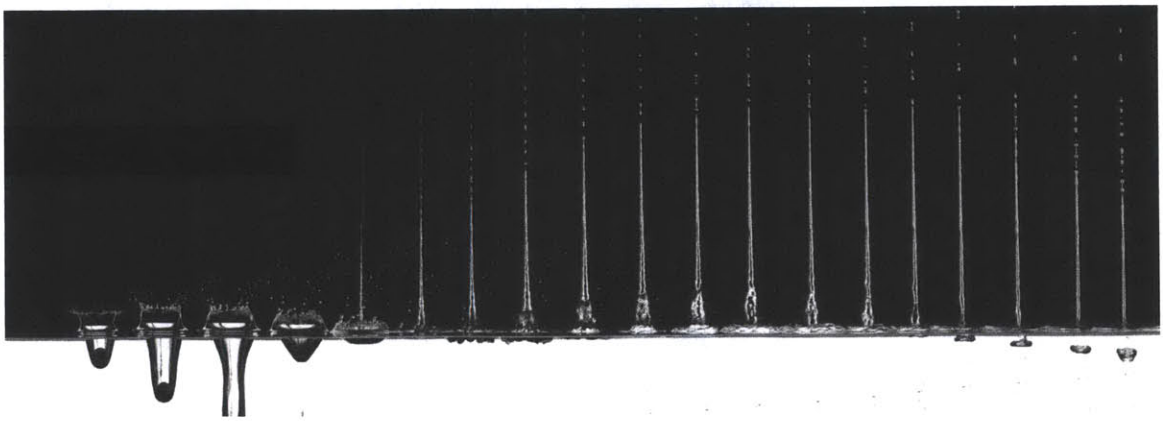

(c) Steel hydrophobic jet, 24 cm

Figure 3-11: Jets formed from impact of hydrophobic spheres are shown. All three types of spheres fell from a height of 24 cm ($Fr = 4.35$). The time between images is 20 milliseconds.

momentum, but the measurements obtained are most likely skewed because of the imperfection. However, the jet in the ceramic case also reaches the highest height of the three, so any energy contributing to the horizontal velocity in the jet is most

likely not significant to jet height in comparison to imperfect surface conditions of the sphere. The acrylic jet has the lowest maximum height of the three. In all cases, just as in Figure 3-6, droplets begin to break off from the tip of the jet, giving the continuous jet a near constant height for some time before the entire jet breaks up. The final breakup of the jet into multiple droplets occurs as the jet is falling back to the free surface.

As a result of the Worthington jet falling back into the fluid, we see in all of the cases in Figure 3-11 a bubble that descends from the free surface in the last five frames of each sequence. This bubble forms at the surface when air is entrained by the fluid column falling into the free surface. It then descends as it is pushed down by the fluid flow. It is important to note that this bubble forms at the same time for each of these three cases, and is therefore independent of mass ratio. All three jets also reach their maximum height (the height which is maintained for some time by the gradual breaking off of individual droplets) at about the same time.

In the next comparison, shown in Figure 3-12, different values of the Froude number are compared for the acrylic hydrophobic sphere. Figure 3-12(a) shows the sphere at $Fr = 2.35$, Figure 3-12(b) shows $Fr = 4.35$, and Figure 3-12(c) shows $Fr = 5.32$. Time between each image is $20ms$. There is no surface closure at any of these Froude numbers for the acrylic case. Here, it is clear that the maximum height of the $Fr = 2.35$ case is much lower than the other two cases, but it is difficult to determine by visual inspection which of the higher two Froude number cases attains a higher height.

One clear difference between the sequences in Figure 3-12 is the time at which the maximum heights are reached. The region where the constant break off of individual droplets occurs is delayed in time as Froude number increases. In Figure 3-12(a), where $Fr = 2.35$, the maximum height region appears to begin in the eighth frame and ends just after the tenth. For the case where $Fr = 4.35$, the region of maximum height occurs between the tenth and fifteenth frames. Finally, for the highest Fr case in Figure 3-12(c), the region occurs between frames twelve and fifteen.

Full breakup of a large portion of the jet in the $Fr = 2.35$ case does not occur

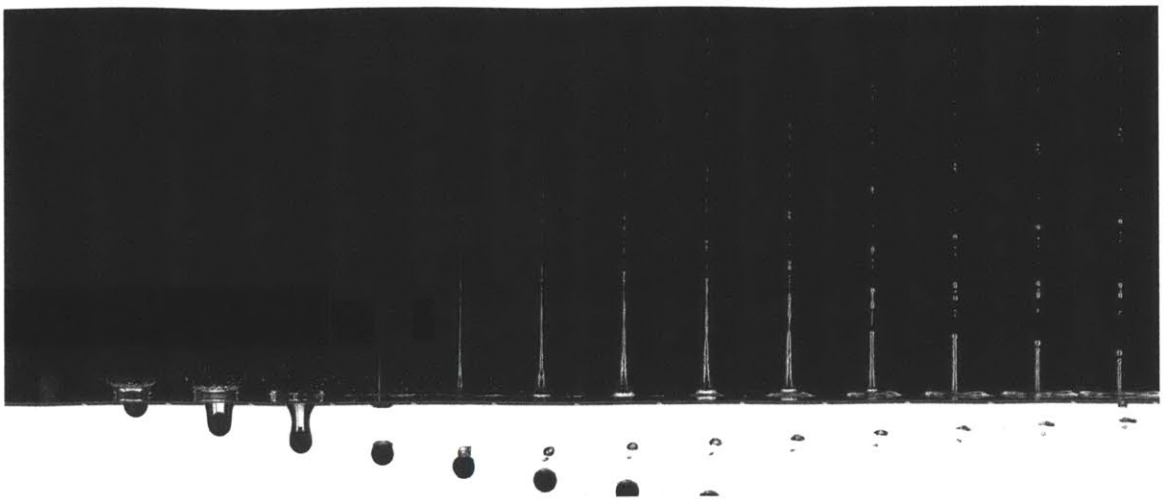

(a) Acrylic hydrophobic jet, 7 cm

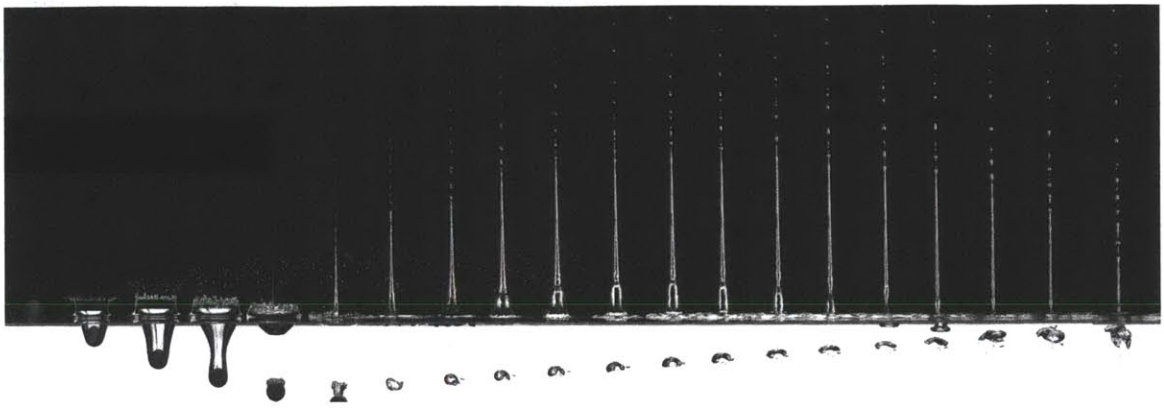

(b) Acrylic hydrophobic jet, 24 cm

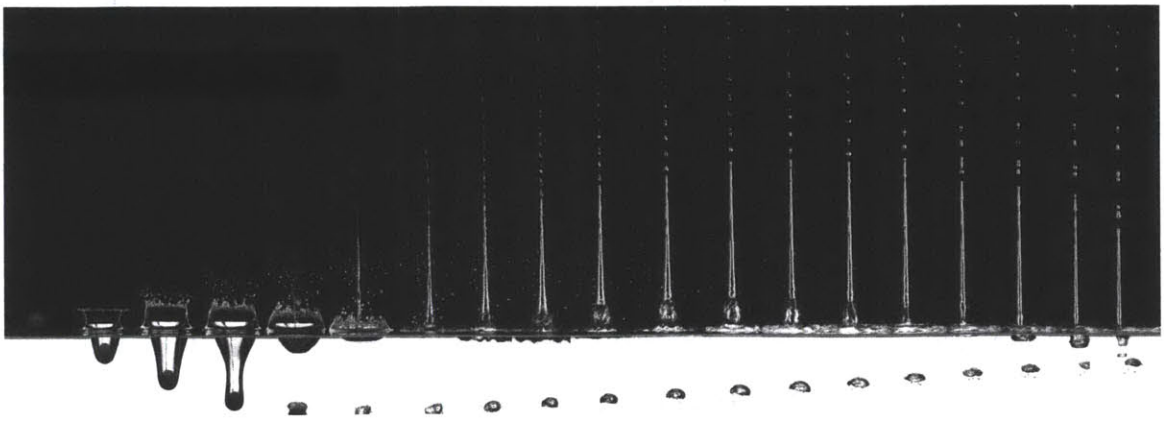

(c) Acrylic hydrophobic jet, 36 cm

Figure 3-12: Jets formed from impact of hydrophobic acrylic spheres are shown. In (a), the sphere fell from a height of only 7 cm ($Fr = 2.35$). The drop height for (b) was 24 cm ($Fr = 4.35$), and for (c) was 36 cm ($Fr = 5.32$). The time between images is 20 milliseconds.

because the jet has a low velocity, and therefore falls back to the free surface before the breakup event. Breakup of the $Fr = 4.35$ jet occurs in the twentieth and final frame in the sequence shown in Figure 3-12(b). The breakup event for the highest Froude number case is not present. In this case, as with the lowest Froude number case, the entire continuous liquid jet falls back to the free surface.

The timing of the fall of the bulk of the jet back to the free surface, as indicated by the bubble of entrained air that is pushed below the free surface, is visible in each of the cases presented in Figure 3-12. This bubble first appears in the fourteenth, sixteenth, and seventeenth frames, respectively, for the three Froude numbers. The time duration of the jet is thus dependent on the Froude number, which higher impact speeds producing jets that remain above the free surface for longer periods of time before they fall back into the fluid.

As a final comparison, Figure 3-13 compares the hydrophilic and hydrophobic cases for a ceramic sphere at a Froude number of 4.86. The time between each frame is 10 ms in both cases. The difference between the two sequences is vast, and by comparing them side-by-side, it is possible to get a better sense of the difference in scale between the two.

Results of the experiments have been presented in the form of raw images, and general observations have been made. Further discussion of the results, including development of scaling laws and parameter characterization, will be given in Chapter 4.

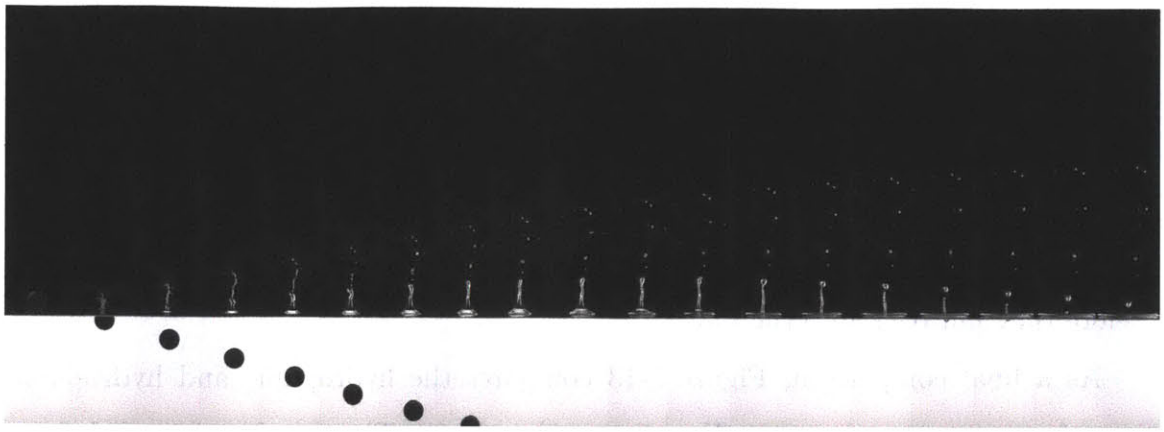

(a) Ceramic hydrophilic jet, 30 cm

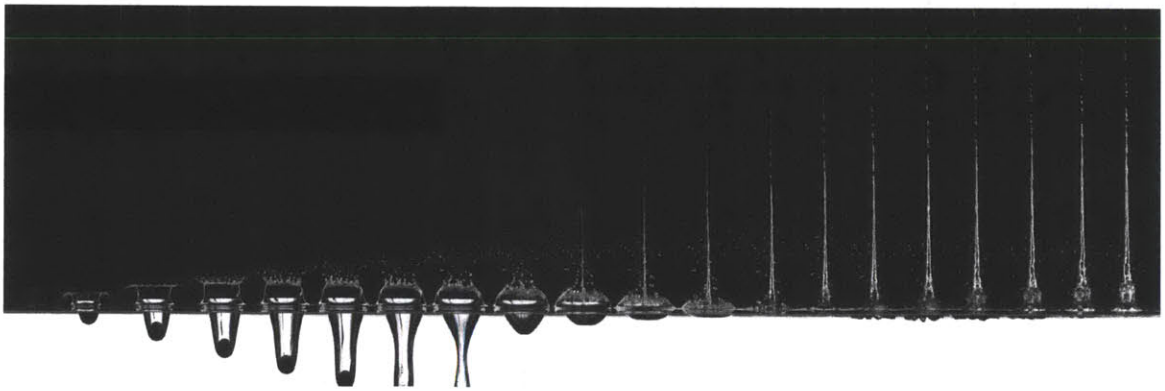

(b) Ceramic hydrophobic jet, 30 cm

Figure 3-13: Jets formed from impact of ceramic spheres with $Fr = 4.86$ are shown. (a) shows the impact of a hydrophilic sphere, while (b) shows the impact of a hydrophobic sphere. The time between images is 10 milliseconds.

Chapter 4

Discussion

As in the Results chapter, this chapter is divided into hydrophilic and hydrophobic sections. Data from all cases is presented to clarify the trends observed in Chapter 3, and explanations for these trends, based on the physical parameters and dynamics of the situation, are given. Focus is on the characteristics of the Worthington jets that have been discussed thus far: maximum height and time to breakup of the first and second hydrophilic jets, and maximum average height, time to maximum height, time to fall, and time to surface closure for hydrophobic cases.

In addition to the Froude number (describing the ratio of inertial to gravitational forces), which was used as a controlled parameter to organize the experiments in this study, other dimensionless quantities are important for explaining the dynamics of the Worthington jet formation and breakup for each case. These additional parameters are the Weber number, Ohnesorge number, and Bond number. They are defined as follows:

$$We = \frac{\rho V_0^2 D_{drop}}{\sigma}$$

$$Oh = \frac{\mu}{\sqrt{\rho D_{drop} \sigma}}$$

$$Bo = \frac{\rho g D_{drop}^2}{\sigma}$$

The Weber number describes the ratio of inertial forces to surface tension effects, the Ohnesorge number compares viscous and surface tension forces, and the Bond

number compares gravitational and surface tension effects. The following values are used for the fluid constants: $\rho = 1000\frac{kg}{m^3}$, $\mu = 1 \times 10^{-3}\frac{kg}{m \times s}$, and $\sigma = 0.072\frac{N}{m}$. The gravitational constant is $9.816\frac{m}{s^2}$.

Note that the length scale in each of these quantities is no longer the diameter of the sphere, but rather D_{drop}, the diameter of droplets ejected from the tip of the jet. Upon inspection of the data, the drop size of each type of jet (the first and second jets in the hydrophilic cases and the jet in the hydrophobic cases) were found to be constant. The velocity used in the calculation of the Weber number, V_0, does not refer to the velocity of the sphere on impact, U_0, that was used for finding Fr. V_0 instead refers to the velocity of the fluid as it enters the Worthington jet.

It is impossible to determine the quantity of V_0 without Particle Image Velocimetry (PIV), which is also extremely difficult given the configuration of the jet and the sphere. As a result, the velocity at the entrance to the jet must be found by other means. However, a quantity that can be easily measured is the velocity of the tip of the jet (and of the droplets ejected from the tip). If the fluid particles in the tip of the jet can be assumed to move with the same velocity as the jet tip and the droplets themselves, then the fluid velocity at the entrance to the jet can be found using Bernoulli's equation for steady flow:

$$\frac{1}{2}\rho U_{drop}^2 + \rho g h_{avg} = \frac{1}{2}\rho V_0^2$$

where U_{drop} is the measured velocity of the tip of the jet, and h_{avg} is the average height of the Worthington jet in the frames used to measure that velocity. This equation measures the height of the jet from the free surface, hence the missing gravitational potential term from the right side. If, during the sequence from which the measurement was taken, a droplet breaks from the end of the jet, the droplet is tracked rather than the jet tip in subsequent frames. This assumes that the velocity of the droplet is equal to the velocity of the jet tip, neglecting any energy that the fluid in the droplet may have lost due to the break off. Once the value of V_0 is obtained from these measurements and the use of the Bernoulli equation, the values of We for

each case can be determined.

4.1 Hydrophilic Cases

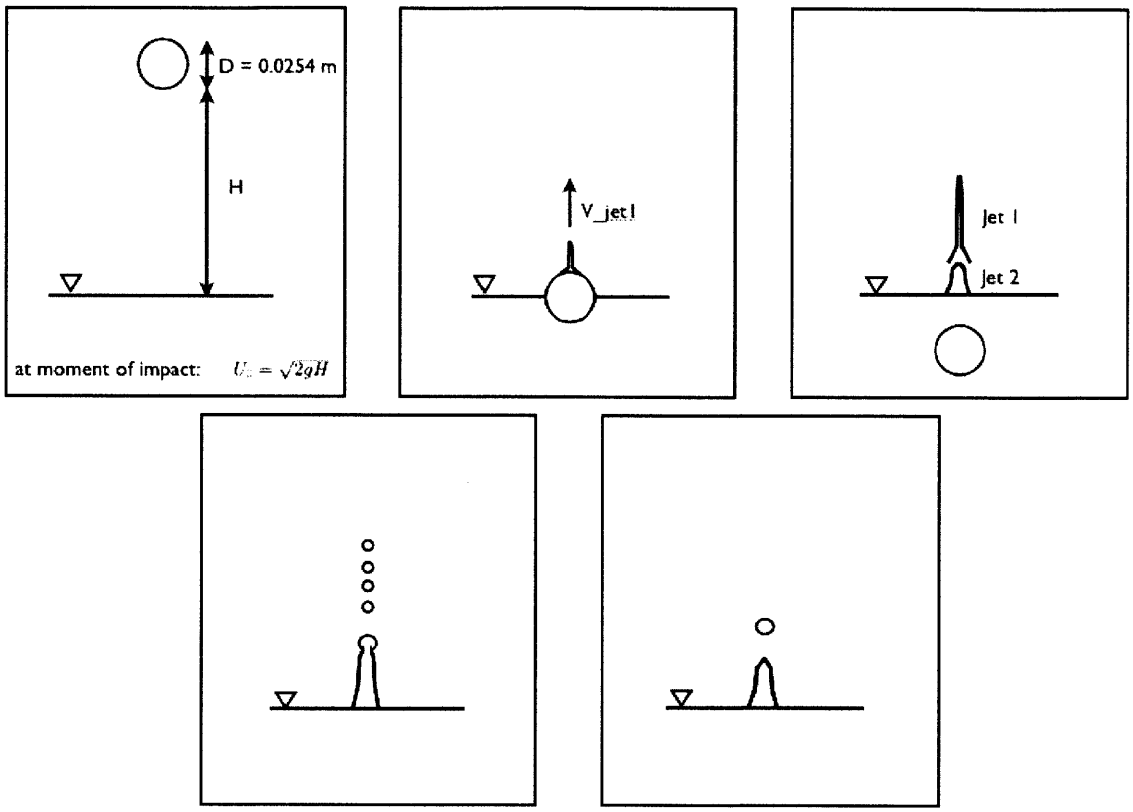

Figure 4-1: The stages of hydrophilic sphere impact and Worthington jet evolution are shown.

The evolution of the Worthington jet formed from the impact of hydrophilic spheres ($\theta \leq 70^o$) with the free surface can be broken into several stages. These stages are illustrated in Figure 4-1. The first frame represents the setup of the experiment, with the sphere stationary at some distance, H, above the free surface. This height is used to determine the Froude number for each case. In the second frame, the sphere has impacted the surface, but is not yet fully submerged, and the first Worthington jet is seen already traveling vertically. The third frame shows some time later when the sphere is fully submerged. Here, the first jet is still seen intact, and the second, slower Worthington jet is also visible. The fourth frame in the series

represents the breakup of the first jet into uniform droplets, and the final frame shows the breakup of the second jet, with the ejection of just one droplet from the tip of the jet. The diameter of all droplets will be referred to as D_{drop}; however, it is important to note that the value of D_{drop} is different for the two Worthington jets formed in the hydrophilic case.

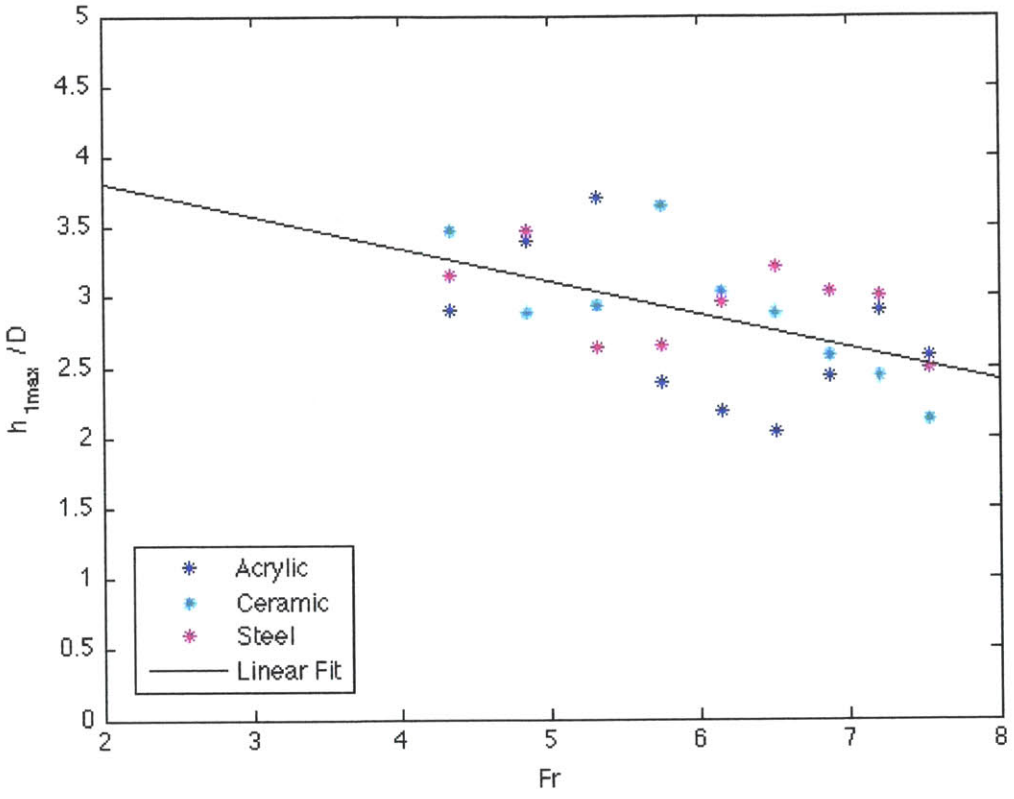

Figure 4-2: The maximum heights of the first Worthington jet in the hydrophilic cases are shown. Heights are non-dimensional in terms of diameter of the spheres, which are all $2.54cm$. The linear trend shows a slope of -0.2334.

4.1.1 Worthington Jet Heights

The first characteristic of the Worthington jet formed from the impact of hydrophilic spheres under review is the maximum height of the first and second jets. The first jet reaches its maximum height just before breakup occurs. After breakup, the remnants of the jet continue to move upward with some velocity, but eventually the entire

jet breaks into droplets. The measured heights of the first jet are shown in non-dimensional form in Figure 4-2. The heights are non-dimensionalized by the diameter of the spheres, which is constant for all cases. A slight downward trend with respect to Froude number is apparent. The spread of the data, however, lends to uncertainty. All heights are within 1 diameter of the mean, and there is not evidence of dependence of maximum height on the mass ratio of the sphere.

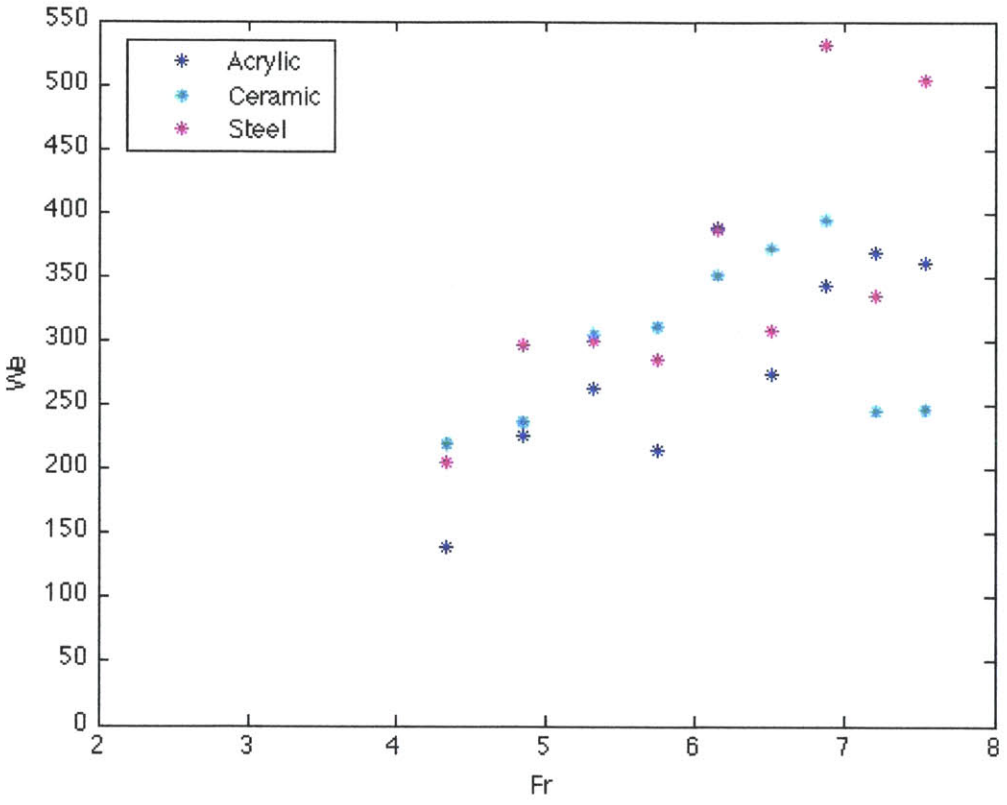

Figure 4-3: The Weber number corresponding to the first Worthington jet in the hydrophilic cases is plotted against the experimental Froude number.

The Weber number for the first Worthington jet formed in the hydrophilic cases is plotted against the Froude number in Figure 4-3. There is a vague linear dependence of Weber number on Froude number, with no apparent dependence on mass ratio. The correlation is not very strong, but the general trend indicates that as the impact velocity of the sphere increases, the initial velocity of the first jet also increases. Considering the dependence of Weber number on Froude number, and the independence

of the maximum heights of the first jets formed by hydrophilic spheres on Froude number, it is not surprising that the maximum height of the first jet is also independent of Weber number. This was confirmed graphically, but the plot is not included here. The evolution of this first jet is most likely more affected by instabilities in the fluid upon initial impact of the sphere than on the pure energy transferred to the fluid by the sphere.

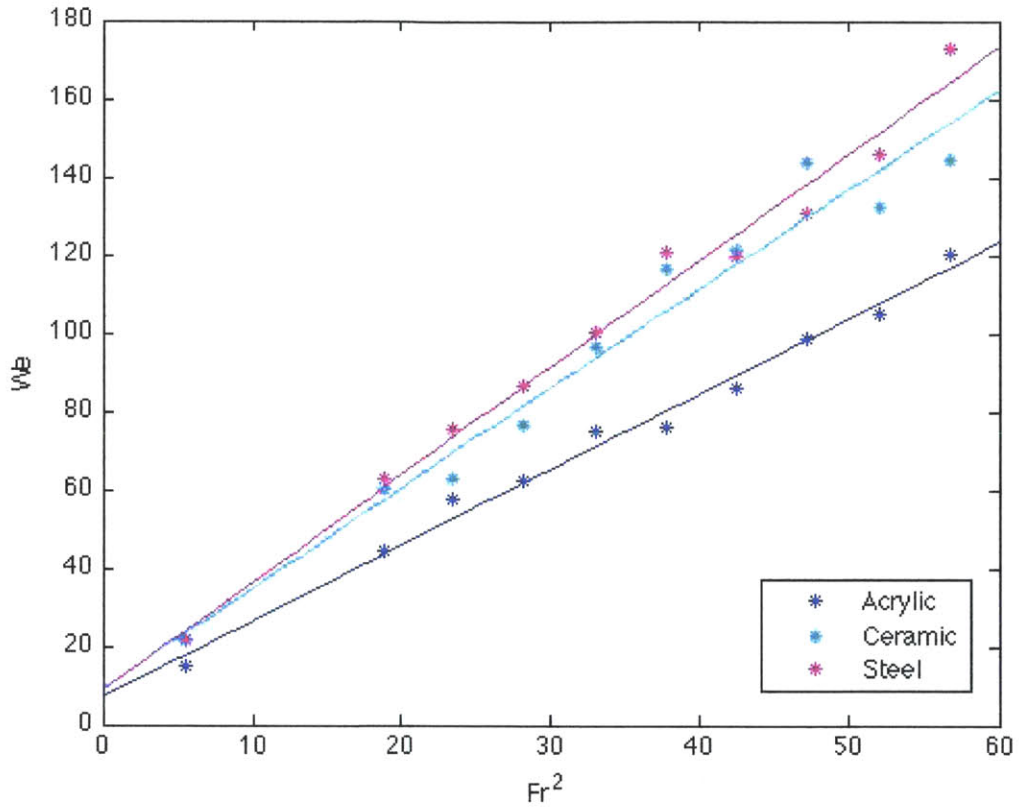

Figure 4-4: The Weber number describing the second Worthington jet in the hydrophilic cases is plotted against the square of the experimental Froude number.

The second Worthington jet, being much more stable than the first, is expected to have stronger dependence on the Weber number. The Weber number for the second jet formed in hydrophilic cases is plotted against the square of the Froude number in Figure 4-4. Here, there is a clear dependence of the velocity of the second jet on the impacting Froude number of the sphere. In contrast to the first jet, however, the linear relationship is to the square of the Froude number, with a proportionality constant

of 1.932 for the acrylic cases, 2.547 for ceramic, and 2.737 for steel. Therefore, the mass ratio of the sphere is also important in determining the Weber number of the second jet, with proportionality increasing with increasing mass ratio.

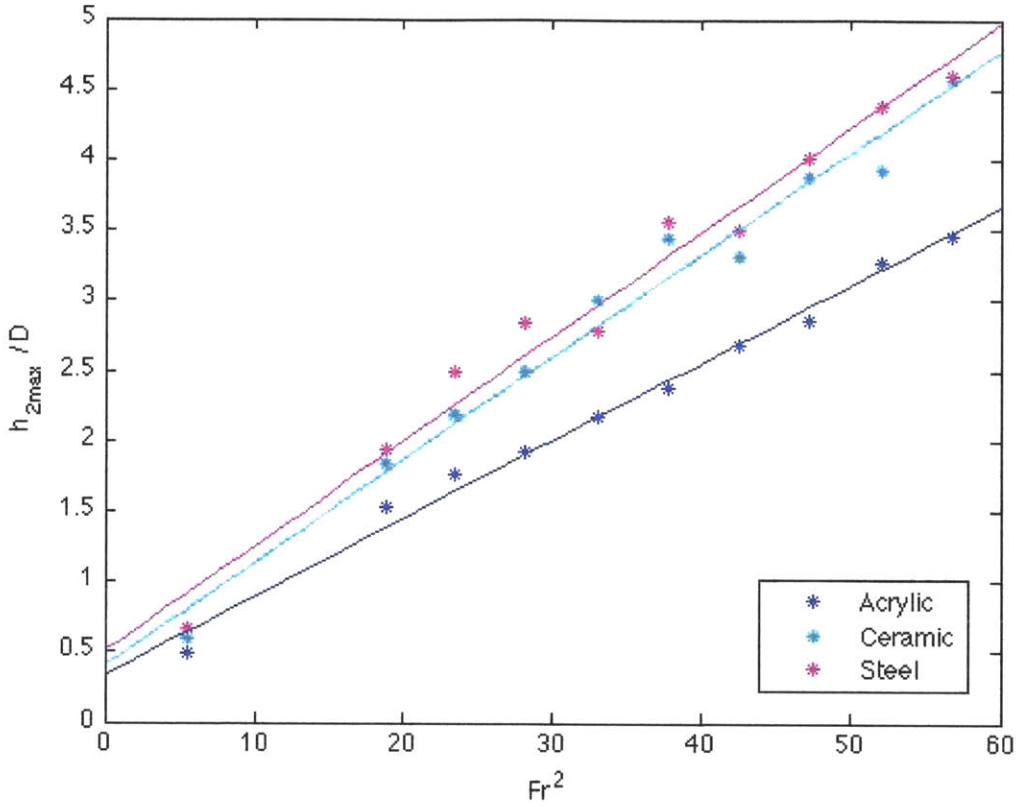

Figure 4-5: The maximum heights of the second Worthington jet in the hydrophilic cases are shown. Heights are given non-dimensionally with respect to the sphere diameter, which is a constant $2.54cm$ for all cases. Maximum heights increase linearly with Fr^2 for each mass ratio.

Next, the heights reached by the second Worthington jet are examined for correlation to the Froude and Weber numbers for the jet. The maximum non-dimensional heights reached by the second hydrophilic jets are plotted against Froude number in Figure 4-5. The maximum height of the jet, h_{2max}, tended to occur just before breakup. These data are much more organized when compared to that for the height of the first jet, and bear a striking resemblance to the data plotted in Figure 4-4. The linear dependence of the height obtained on the square of the Froude number is clear, with the solid lines indicating the best fit line for each mass ratio, and mass ratio is

still recognized as a relevant parameter, with increasing m^* leading to an increase in maximum height of the second jet.

The correlation between the dependence of the second jet's Weber number and of the maximum height on the square of the Froude number becomes clear when $\frac{h_{2max}}{D}$ is plotted against Weber number. In Figure 4-6, mass ratio is not a factor in the linear relationship between jet height and We. It is this proportionality that results in the similarity of Figures 4-4 and 4-5.

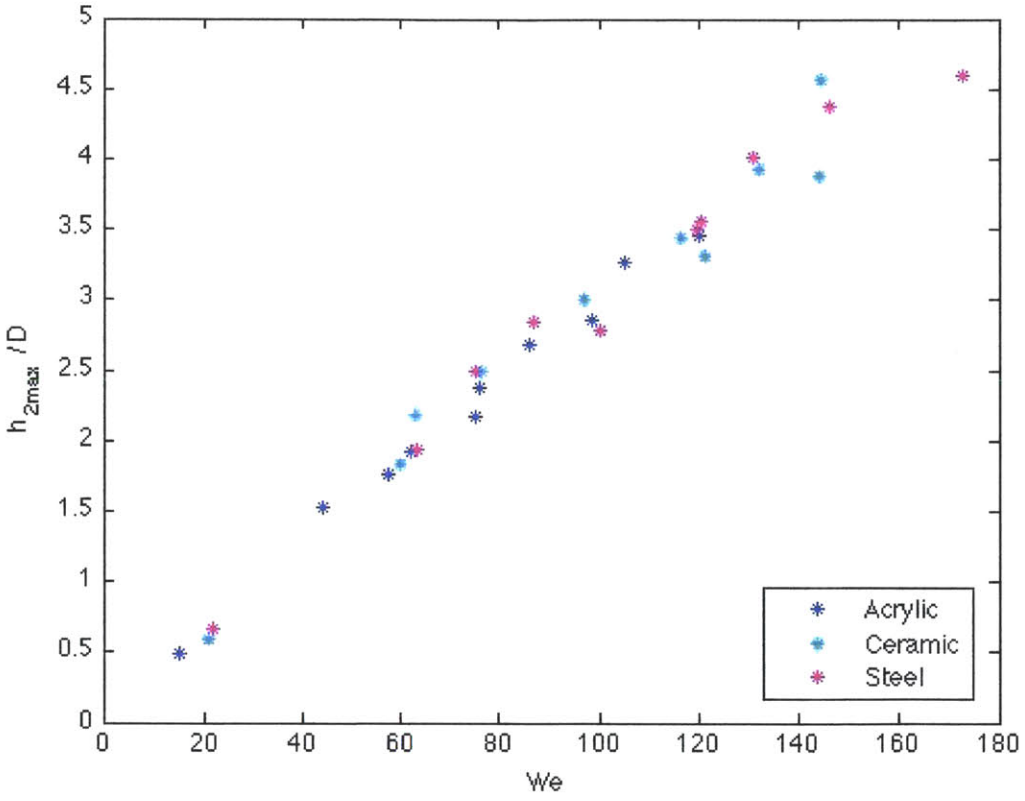

Figure 4-6: The maximum heights of the second Worthington jet in the hydrophilic cases are shown. Heights are given non-dimensionally with respect to the sphere diameter, which is a constant $2.54cm$ for all cases. Maximum heights increase linearly with Fr for each mass ratio.

The scale of the y-axis in both Figures 4-2 and 4-5 is the same, showing heights of the first and seconds jets from 0 to 5 diameters. The height of the first jet is 3 diameters for all Froude numbers, while the height of the second jet ranges from $\sim$ 0.5 diameter at the lowest Froude number to almost 5 diameters at $Fr = 7.53$.

This indicates that the height of the second jet exceeds the maximum height of the continuous first jet in higher Froude number cases.

4.1.2 Bond and Ohnesorge Numbers

The size of the droplets formed by the breakup of the first and seconds jets, which are important for the calculations of the Bond and Ohnesorge numbers, are easily measured. The droplet size depends only on which of the two Worthington jets produced it, resulting in a constant Bo and Oh for the first and second jets. The data indicate that $D_{drop} \approx 3.2mm$ for the first jet, and $D_{drop} \approx 9.3mm$ for the second jet. The resulting Bond and Ohnesorge numbers are summarized in Table 4.1.

Table 4.1: Bond and Ohnesorge Numbers from Hydrophilic cases

Jet Number	Bond Number	Ohnesorge Number
First	1.325	2.1×10^{-3}
Second	11.932	1.2×10^{-3}

The Ohnesorge number is $\ll 1$ for both jets, indicating that viscosity is not an important parameter. The Bond number, however, is $\sim O(1)$ for the first jet and $\sim O(10)$ for the second jet. This shows that gravity cannot be neglected in either jet, but that it is more influential in the second jet than in the first.

4.1.3 Time to Breakup

The next characteristic notable for discussion is the time to breakup of both the first and second jets. Figure 4-7 shows these times non-dimensionally, such that $t^*_{breakup} = \frac{t_{breakup}U_0}{D}$. U_0 is, again, the velocity of the sphere on impact with the free surface in m/s, and D is the diameter of the sphere in m. The non-dimensional breakup times are plotted against Fr, so the impact velocity is included in both axes. The non-dimensional time to breakup of the second jet is linear with Fr, and t^*_{break} of the first jet is constant. Neither value has any dependence on mass ratio.

The non-dimensional breakup times of the first jet have a mean value of 4.42 with a standard deviation of only 0.63, or 14%. The constant value of $t^*_{breakup}$ with

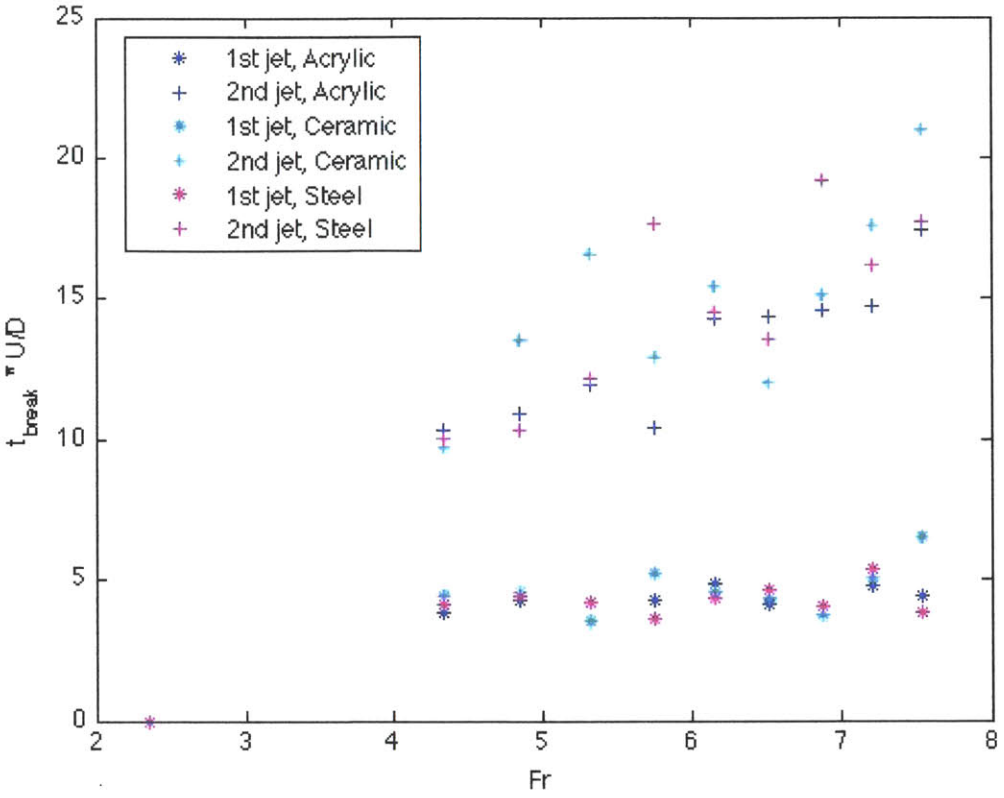

Figure 4-7: Non-dimensional time to jet breakup is shown for both Worthington jets emitted from hydrophilic impacts. With the dimensionless scale, the time to the first breakup is now constant, and the time to the second breakup increases linearly with increasing Fr

Fr indicates that as the velocity on impact, U_0 increases, the dimensional time to breakup must decrease proportionally. This decrease in breakup time can be linked to an increase in the instability of the first Worthington jet, proportional to the amount of energy transfered to the fluid upon first impact of the sphere with the free surface. Again, because the Weber number and Froude number are linearly related to each other, the non-dimensional time to breakup for the first jet is also independent of Weber number, as shown in Figure 4-8. Figure 4-8 also shows the time to breakup of the second Worthington jet plotted against the value of the Weber number, and here a linear dependence of the dimensionless time on We is apparent.

As expected, the non-dimensional breakup times for the second jet follow a linear trend whether plotted against We or Fr, so as impact velocity (and, subsequently,

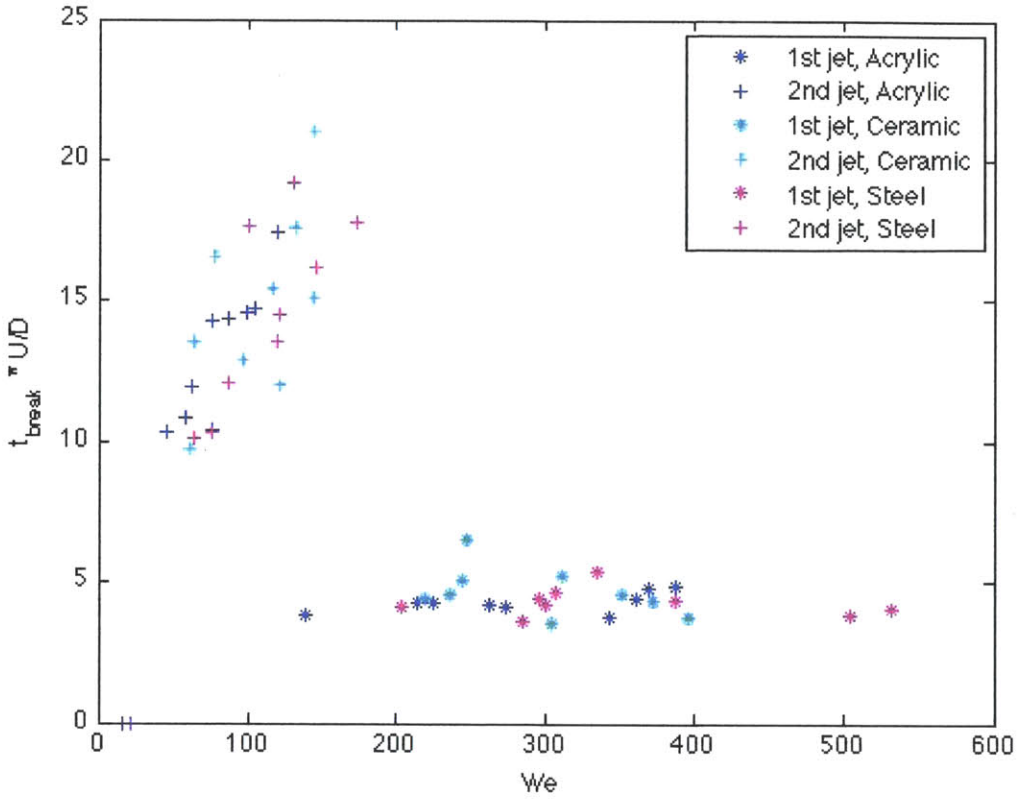

Figure 4-8: The dimensionless time to breakup of both the first and second Worthington jets formed in the hydrophilic case are plotted against Weber number.

V_0) increases, dimensional time to breakup remains constant. This suggests a transfer of energy or momentum to the fluid that is independent of the sphere's velocity.

4.1.4 Energy Transfer

The energy transferred to the fluid by the sphere was estimated using the velocity of the sphere at times following impact compared to U_0. The initial energy of the sphere (just before impact) is known to be

$$KE_{sphere} = \frac{1}{2} m_s U_0^2,$$

where m_s is the mass of the sphere. Here, all energy in the system is described by this kinetic term for the sphere, with no contribution of gravitational potential energy at

the free surface. Using Matlab® to track the sphere under the surface, the velocity of the sphere for each subsequent depth could be found, and the sphere's energy at each time following impact approximated. Energy transferred to the fluid is then given as

$$E_{trans} = \frac{1}{2} m_s (U_0^2 - v^2) + m_s g d$$

where v and d are the velocity, in m/s, and the depth, in m, of the sphere after impact, respectively.

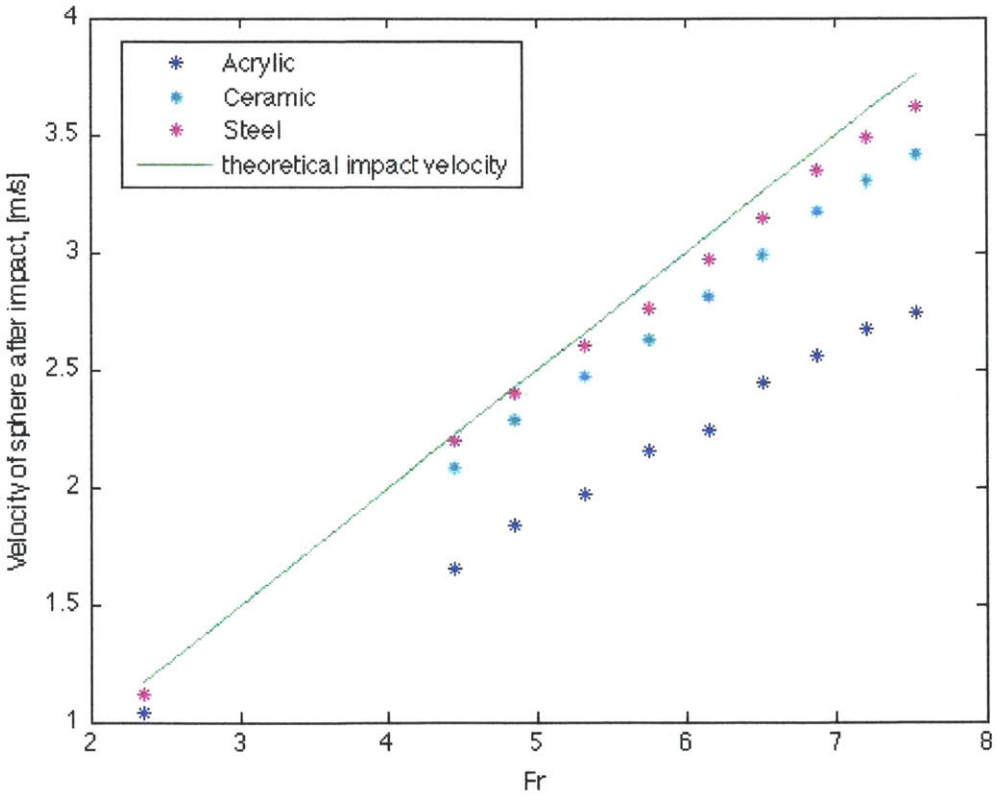

Figure 4-9: Velocities of hydrophilic spheres approximately $10ms$ after impact are shown as a function of Froude number. The green line indicates the impact velocity of the spheres as predicted by theory. The steel spheres retain the most of their original velocity, while the acrylic spheres are significantly slowed by the fluid.

Figure 4-9 shows the velocities of each sphere at each Froude number approximately $20ms$ after impact, after the sphere is fully submerged. These are the velocities used to find the energy transferred by the sphere to the fluid. The solid line

indicates the initial velocities of the sphere at impact due to the force of gravity alone. The decrease in velocity is greater for lower mass ratios, which has been shown in previous works. The velocity lost is also greater for higher Froude numbers, though only slightly.

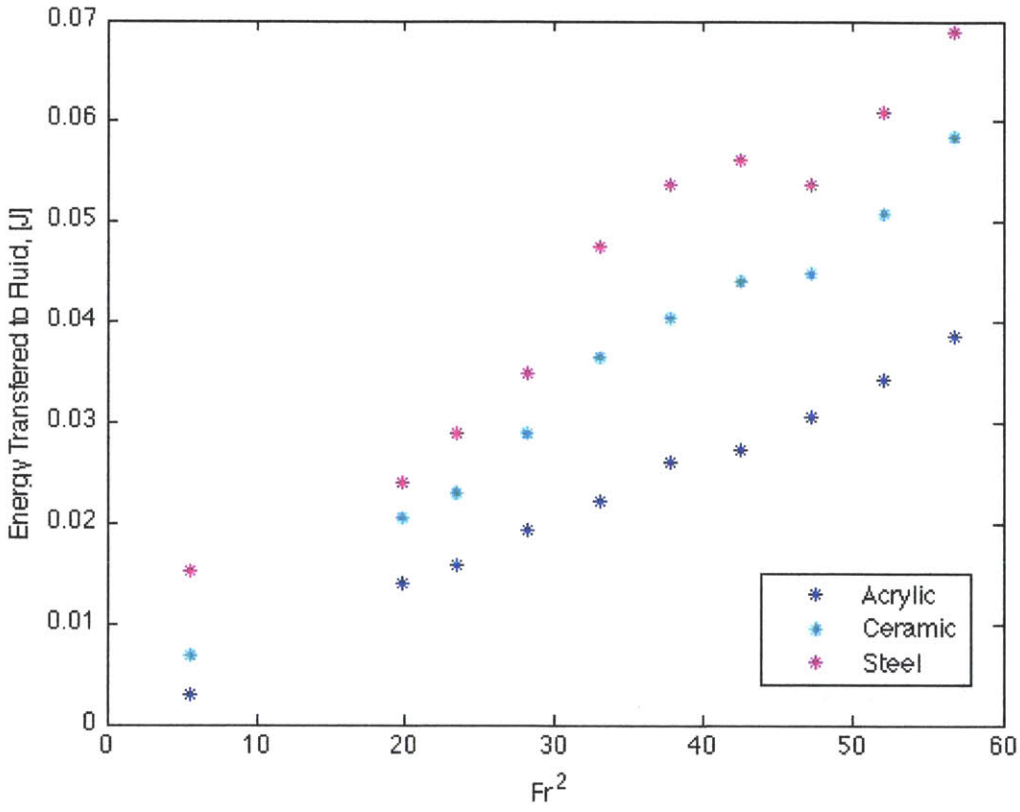

Figure 4-10: Energy transferred to the fluid upon impact is shown to be a linear function of the square of the Froude number, $\frac{U^2}{gD}$.

The energy transferred from the sphere to the fluid after impact is shown in Figure 4-10. The energy, shown in the Figure in *Joules* is plotted not against Fr, but Fr^2. The energy transferred is thus proportional to the square of the velocity of the sphere on impact, which is expected due to the linear relationship between velocity at $20ms$ after impact and U_0 (Fr). Dependence on mass ratio is also evident in this figure, with more overall energy transferred by spheres of higher mass. This might be counter-intuitive, because the spheres with lower mass ratios decelerate more quickly in the fluid, and would thus be expected to lose more energy. However, when the energy

transferred in J is compared to the initial energy of each sphere, the steel sphere loses the lowest percentage of its total initial energy of all three mass ratios, while the acrylic loses the highest percentage of its initial energy to the surrounding fluid.

The dependence of transferred energy on the square of the Froude number is also promising for comparison to the dependence of the second jet on the square of the Froude number. The transfer of energy to the fluid in the first $20ms$ after impact, with the sphere fully submerged, has a direct impact on the height reached by the second Worthington jet. The first jet's dependence on Froude number demonstrates that the first jet does not have the same dependence on the energy transferred after full submergence of the sphere.

From this information, we can begin to understand how the energy transferred to the fluid during and after impact affects the development of the first and second Worthington jets in the hydrophilic case. Not all of the energy lost by the sphere can be assumed to enter the Worthington jet. Some is lost to viscous forces on the boundary layer of the sphere, in the bulk of the fluid, or even in sound generation.

4.2 Hydrophobic Cases

The formation of the Worthington jet resulting from the impact of hydrophobic spheres ($\theta \geq 90^o$) can be divided into six stages, outlined in Figure 4-11. The first stage is identical to the first stage of the hydrophilic sphere case, with the sphere at rest a height, H, above the free surface. From H, the impact velocity of the sphere is calculated and the Froude number defined.

In the second stage, the difference between the hydrophobic and hydrophilic cases becomes clear, with the formation of the cavity below the free surface. The fluid moves radially outward from the cavity, with no vertical component to the velocity at any point along the cavity wall. In the third stage, the flow has turned to be completely radially inward, and pinch-off occurs at some depth, d_p, below the free surface. The time at which pinch-off occurs is denoted as t_p. The Worthington jet originates from d_p; when the walls of the cavity meet, fluid is forced both upward

and downward. The downward jet is confined by the remaining cavity attached to the sphere, but the upward jet is unimpeded. In the fourth frame, the upward jet is depicted as moving with some initial velocity, V_0. In this study, V_0 will be used to denote the fluid velocity at the entrance to the Worthington jet.

The fifth stage depicts the Worthington jet when it is at its maximum height, shown as h_{avg}. During this stage, droplets are ejected from the tip of the jet such that the continuous portion of the jet maintains an average maximum height. The droplets that are ejected have a measurable diameter and ejection speed, D_{drop} and U_{drop}, respectively. The sixth stage shows the breakup of the majority of the Worthington jet into droplets. In the hydrophobic cases, it was found that all values of D_{drop} are similar to within $2mm$.

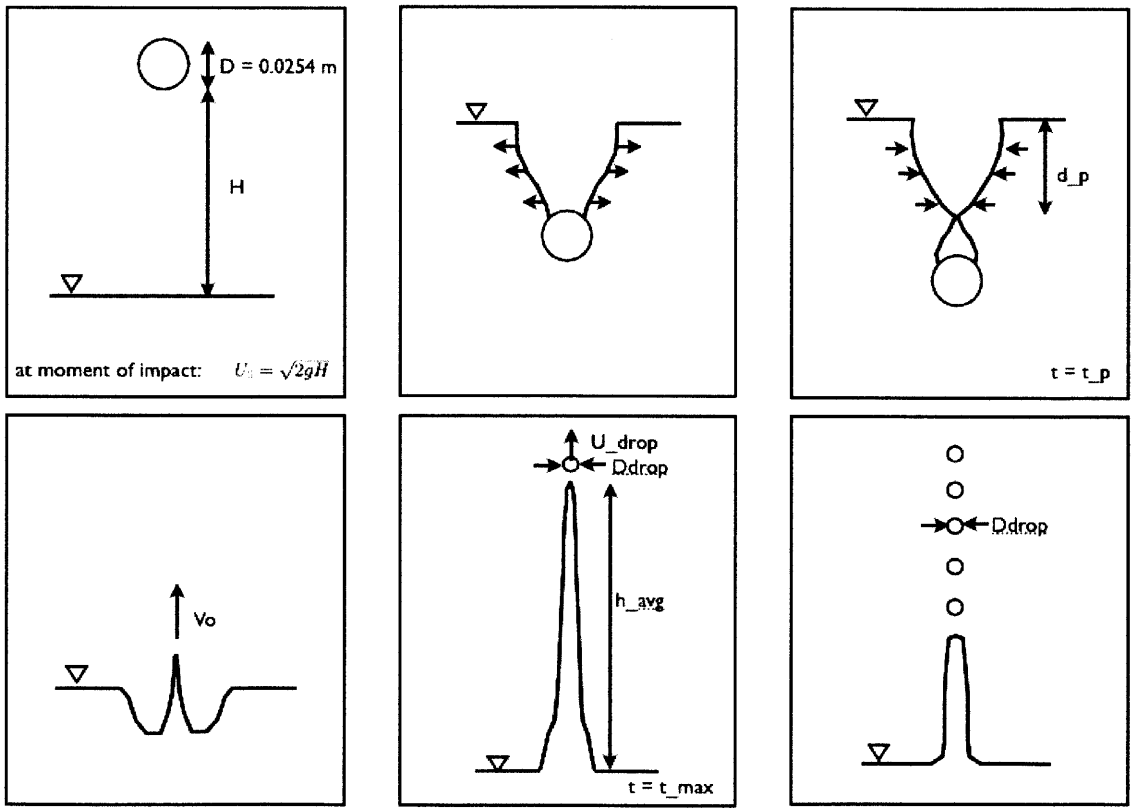

Figure 4-11: The stages of hydrophobic sphere impact and Worthington jet evolution are shown.

Though the formation of an axisymmetric cavity by hydrophobic spheres has been thoroughly studied, certain aspects of cavity dynamics are revisited here to draw

connections between cavity shape and Worthington jet characteristics. The most relevant parameter of the cavity that is examined for this purpose is the depth at which pinch-off occurs, d_p. This parameter is related to the volume of the cavity at pinch-off, which can be compared to a potential energy dependent upon the hydrostatic buoyancy force on the cavity. It is known from previous work on cavity dynamics that mass ratio and Froude number both play a role in the transfer of energy from the sphere to the cavity. In Figure 4-12 the depth at which pinch-off occurs in cases without surface closure are plotted non-dimensionally against $Fr \times m^{*1/4}$, which results in a linear relationship.

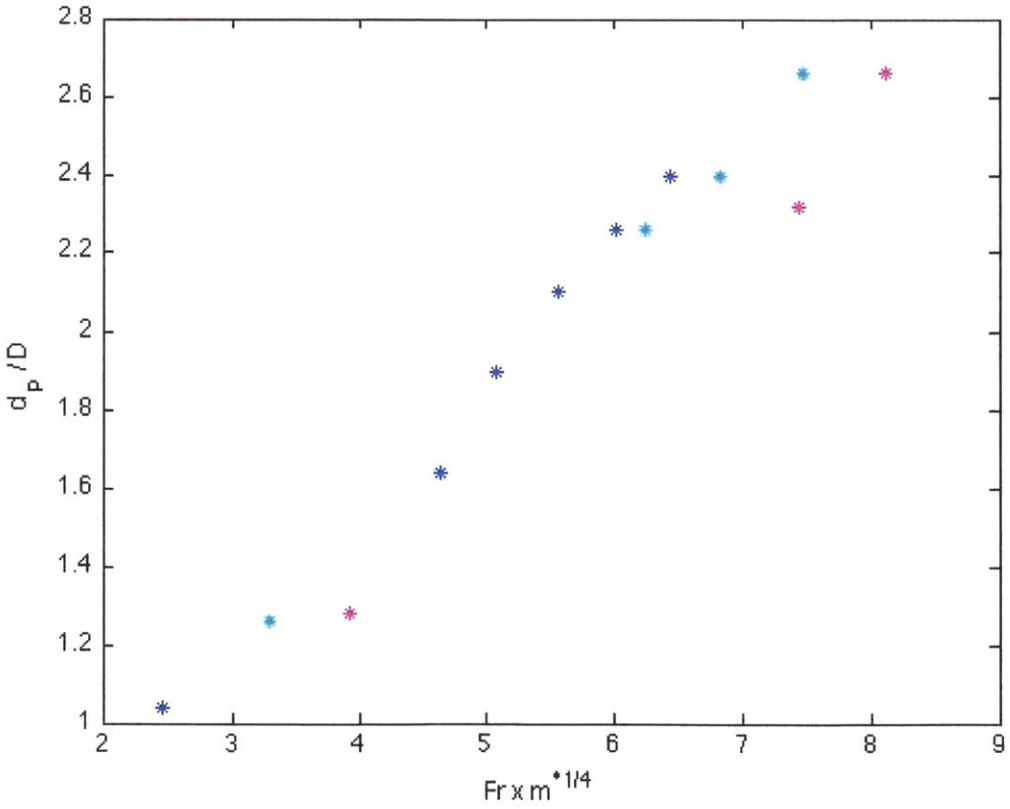

Figure 4-12: Figure (a) scales the non-dimensional depth at which pinch-off occurs with $m^{*1/2}Fr$, and Figure (b) scales $\frac{d_{pinch}}{D}$ with $m^{*1/4}Fr$.

The majority of other relevant information gathered from the data is found during the fifth stage of jet evolution as defined in Figure 4-11. During this time period, the height of the jet, velocity of the tip/droplets, and the diameter of the droplets ejected

are all measured to enable calculation of the Bonde, Ohnesorge, and Weber numbers.

4.2.1 Worthington Jet Heights

The first piece of this puzzle that will be discussed is the height of the Worthington jets, which was recorded with time to give a full description of the lifespan of the continuous jet. These data are shown non-dimensionally in Figures 4-13, 4-14, and 4-15. Heights in meters were normalized by the height above the free surface from which the sphere fell, not the diameter of the sphere. This is important to keep in mind. Figure 4-13 shows each of the acrylic hydrophobic cases. Some Froude numbers are represented twice, by two separate runs. These are the result of instances where the first trial of a Froude number appeared to have been messy or otherwise non-ideal.

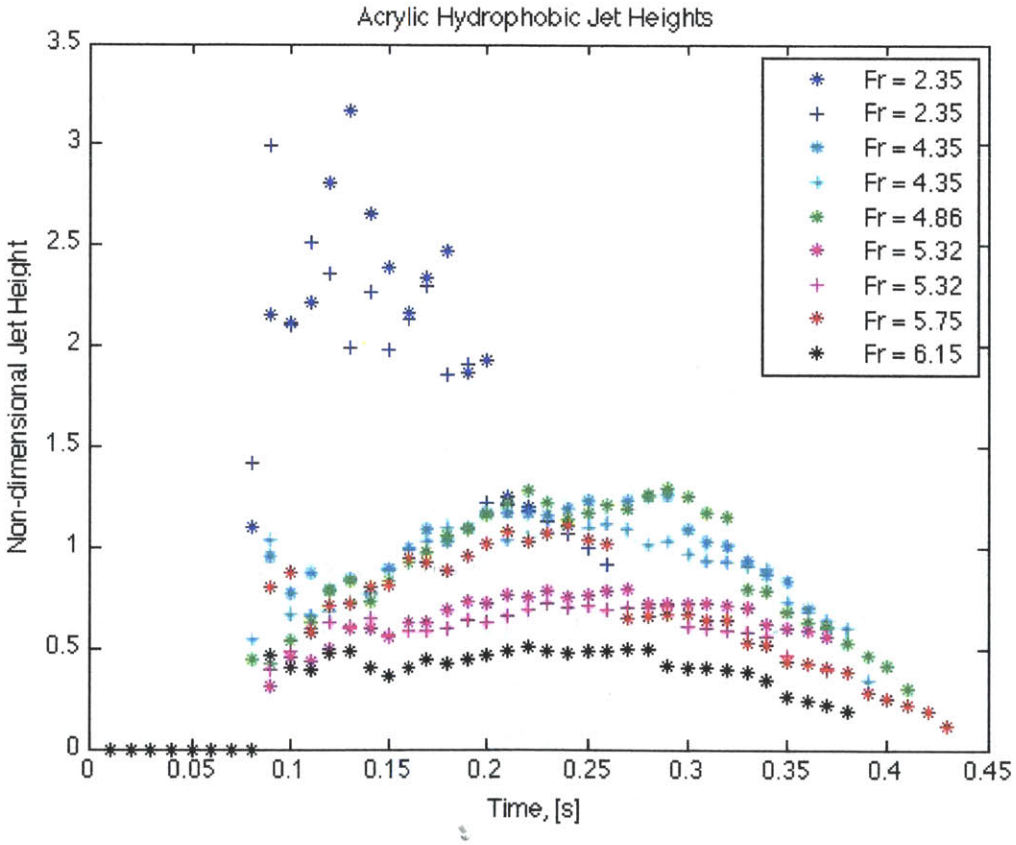

Figure 4-13: The non-dimensional heights of each hydrophobic Worthington jet for the acrylic cases are shown vs. time. Heights are non-dimensionalized by the height from which the sphere fell above the free surface. The data were taken from every fifth frame, or every $10ms$.

All of the jets seem to have roughly the same lifespan with the exception of the $Fr = 2.35$ cases. The Worthington jets for this case reach maximum heights that are three times the height from which the spheres were released. The maximum heights for the other cases are all roughly on the order of the height from which the spheres fell. The jet that reaches the lowest percentage of the sphere's drop height is the $Fr = 6.15$ case, which corresponds to a drop height of $48cm$. For the cases above this Froude number, surface closure prevented measurement of an unobstructed Worthington jet.

Of the acrylic cases that were repeated, there was very good agreement between the two runs. The data in Figure 4-13 seem to suggest that as Froude number increases, the non-dimensional height reached by the resulting Worthington jet decreases. The exceptions to this trend in the acrylic case are the $Fr = 4.86$ and the $Fr = 5.75$ runs. Neither of these cases were repeated because upon visual inspection of the images obtained in those runs, the Worthington jets were very "clean," lacking any features that would suggest that there was slight experimental error. Both of these cases have maximum heights higher than one would expect from the trend suggested, so it is possible that these jets were unusually well-formed, and therefore reached higher maximums than could be repeatedly obtained.

The trend suggested by the data in the acrylic case is further supported by the data in Figure 4-14. Here, the ceramic cases are shown. Only four separate Froude numbers produced Worthington jets which are not impeded by surface closure. Once again, the lifetime of the jets are all on the same order excepting the $Fr = 2.35$ case. Also, the $Fr = 2.35$ case produces the highest maximum with respect to its drop height. Repeated cases are in good agreement. Another interesting note, which was also apparent in Figure 4-13, is the time at which the jets are first measured. At $t = 0s$, the spheres first impact the free surface. The first time at which the Worthington jet is measured in almost every case is $10ms$ after impact. This follows logically from the fact that the time at which pinch-off occurs, t_p, is proportional to the square root of the sphere diameter, and is therefore constant in the cases studied here.

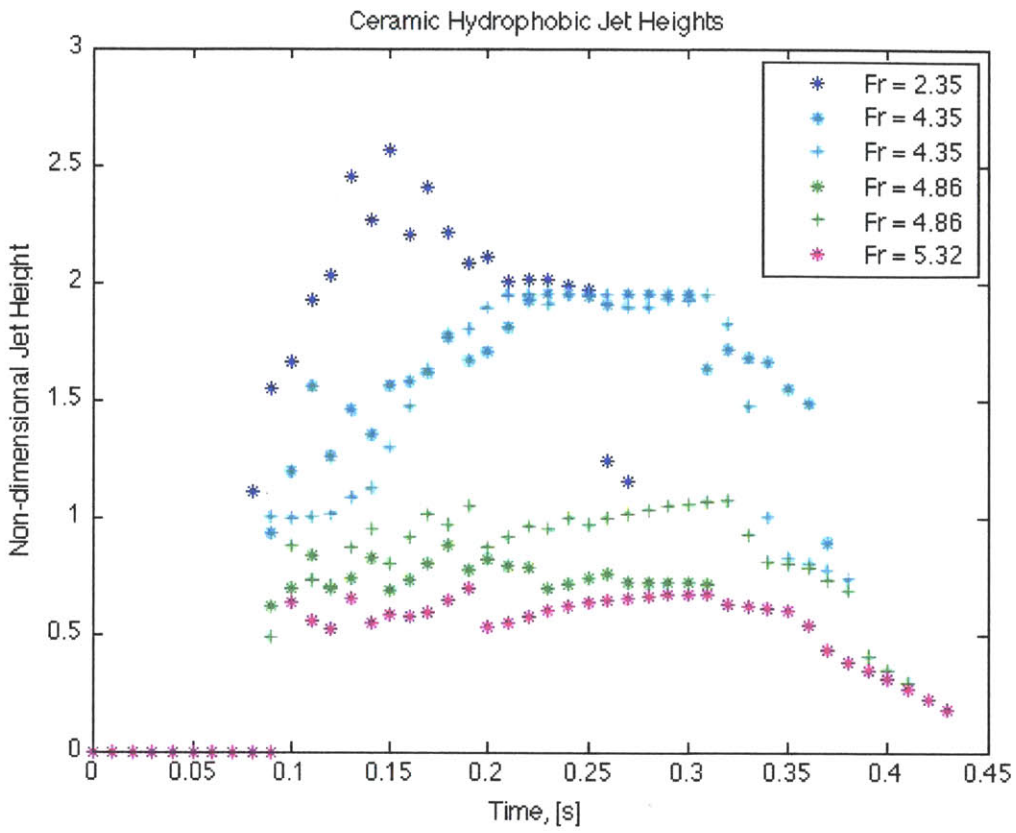

Figure 4-14: The non-dimensional heights of each hydrophobic Worthington jet for the ceramic cases are shown vs. time. Heights are non-dimensionalized by the height from which the sphere fell above the free surface. The data were taken from every fifth frame, or every $10ms$.

The non-dimensional jet heights for the steel sphere cases are shown in Figure 4-15. Here, there are only three Froude numbers studied that result in Worthington jets unimpeded by surface closure. As seen in the acrylic and ceramic cases, the decreasing trend in non-dimensional height with increasing Froude number is apparent, as well as the uniform time of jet formation.

From these data, the average maximum height of the Worthington jets was found. The beginning and end of the time frame in which the jet was at the maximum average height was somewhat arbitrarily deduced. Each case results in a different pattern of breakup at the maximum, so it is difficult to determine precisely when the jet has entered that state. Also measured was the diameter of the droplets ejected from the tip of the jet, D_{drop}, and the velocity of the jet tip (or of the droplets ejected) U_{drop}. As

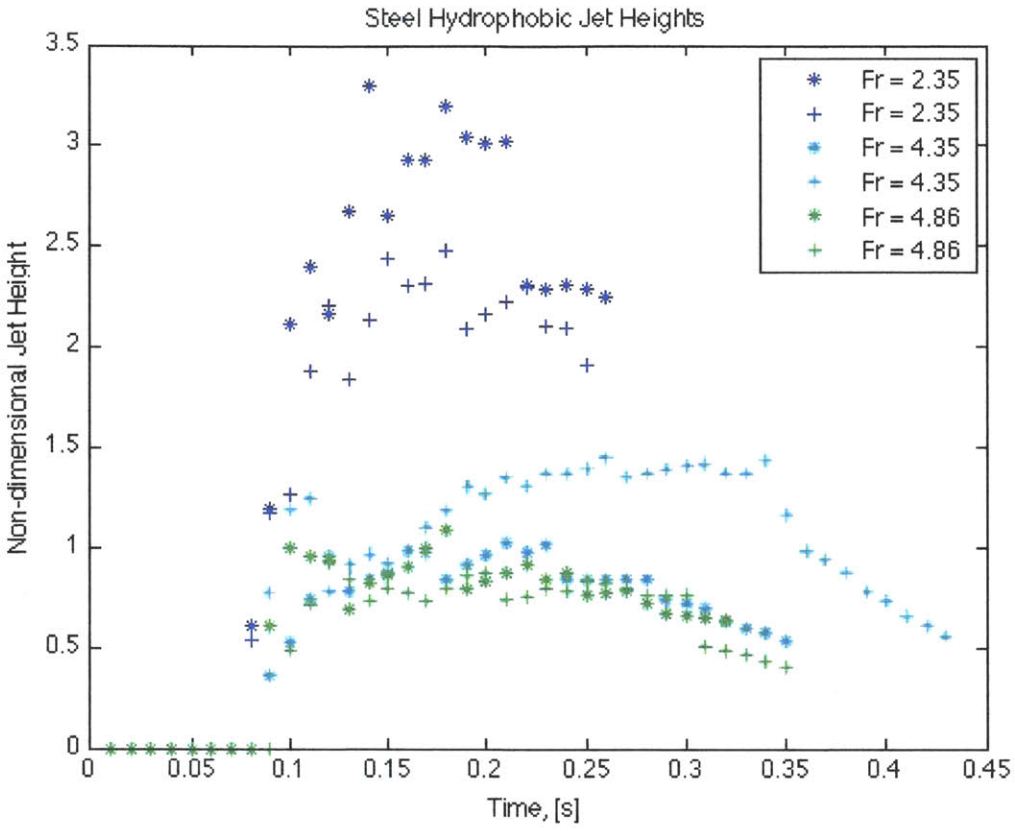

Figure 4-15: The non-dimensional heights of each hydrophobic Worthington jet for the steel cases are shown vs. time. Heights are non-dimensionalized by the height from which the sphere fell above the free surface. The data were taken from every fifth frame, or every $10ms$.

described, this information was used to find the initial velocity of the fluid entering the Worthington jet, V_0, which serves as the velocity scale for the Weber number. The values of D_{drop} were also used to calculate Oh and Bo. The drop diameters for the hydrophobic cases were very uniform, having an average value of $4.5mm$. The resulting Ohnesorge number, therefore, is $Oh = 1.8 \times 10^{-3}$, and the value of the Bond number is $Bo = 2.761$. From this it is clear that, because $Oh \ll 1$, viscosity is not an important factor. The Bond number being $\sim O(1)$, however, indicates that gravity cannot be neglected.

The values of the Weber number calculated are plotted in Figure 4-16 as a function of Froude number. There is evidence of a dependence of We on Froude number, but the experimental error makes it difficult to define it well. It appears that mass ratios

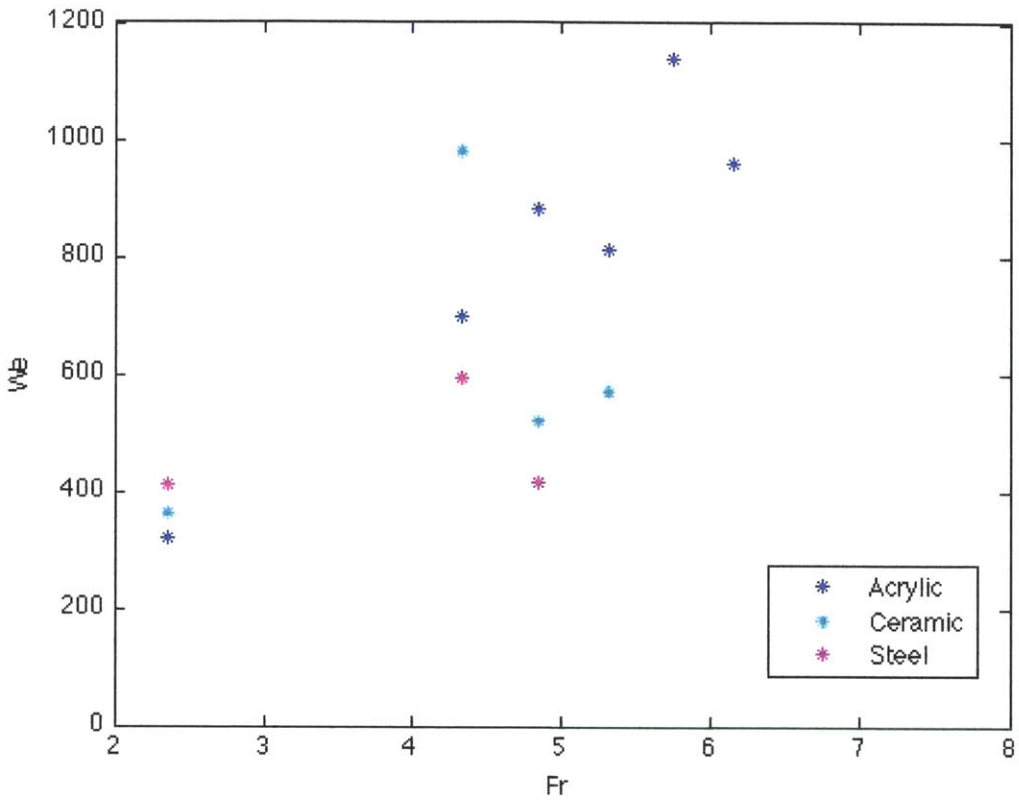

Figure 4-16: The Weber number for the Worthington jets formed by the impact of hydrophobic spheres are plotted against the Froude number of the sphere on impact. The Weber number is based on the initial velocity of the fluid particles entering the jet, which is calculated using information about the velocity and height of the tip of the jet and Bernoulli's equation.

plays no role in determining the Weber number of the jet, but perhaps a linear correlation to Froude number or to the square of the Froude number is present. The precise relationship is difficult to determine.

To attempt to clarify the relationship between the characteristics of the Worthington jet in the hydrophobic cases and the Weber number, the average maximum height, normalized by sphere diameter, is plotted against We in Figure 4-17. Here again, there is a suggestion of a linear dependence, but the spread of the data is not ideal. A linear fit to the data is shown, and most of the heights are within two diameters of this fit. In order to comment on the confidence of the conclusions reached, it is necessary to better understand and quantify the error in the hydrophobic mea-

surements.

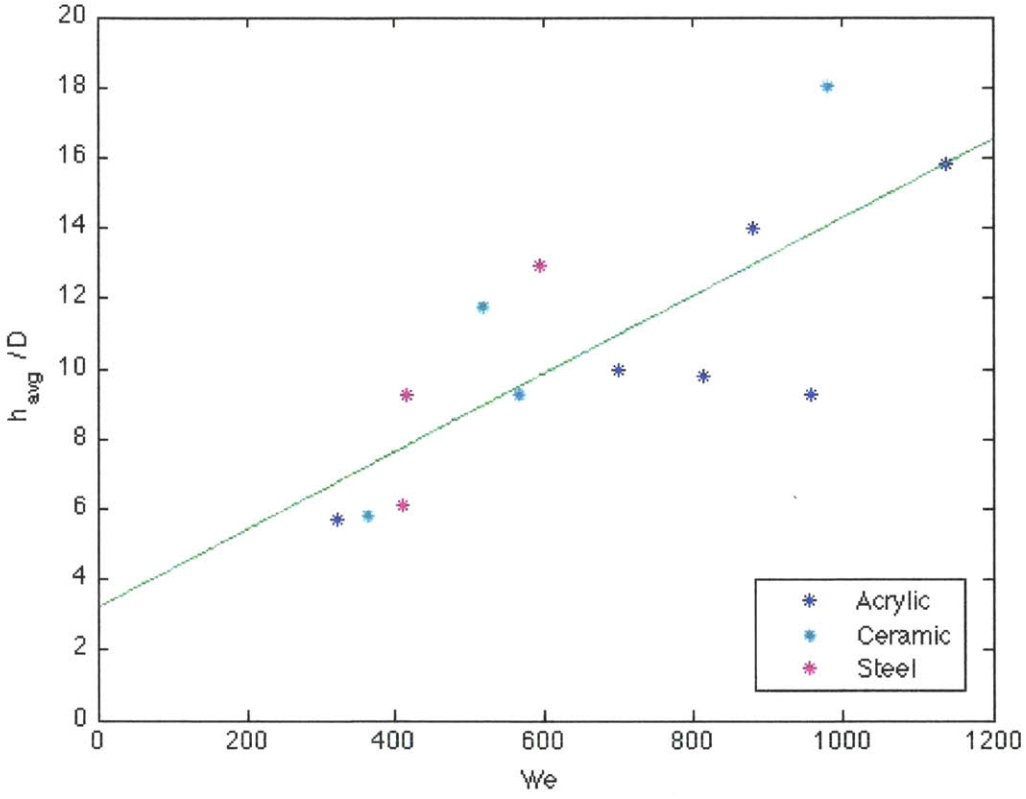

Figure 4-17: Non-dimensional jet heights reached by the hydrophobic cases are shown as a function of Weber number, $We = \frac{\rho V_0^2 D_{drop}}{\sigma}$.

4.2.2 Experimental Error Quantification

As described in Chapter 2, this was accomplished through repeated trials of two cases: acrylic spheres with $Fr = 4.86$ and ceramic spheres, also with $Fr = 4.86$. The heights of the jets were measured with time, and the heights at each time step were averaged for each case. The resulting means are plotted in Figure 4-18. The error bars indicate one standard deviation above and below the mean. The heights are non-dimensionalized by diameter. The solid lines are quadratic fits to the mean heights, starting with the first measured height above the free surface.

The ceramic case produces consistently higher jets than than the acrylic case. The mean values are mostly outside the standard deviation of the other case, though

the standard deviation is $\approx$ 2 diameters. The sample size is still small to reach statistically significant conclusions, but the results are still valuable for estimating the error in the experiment.

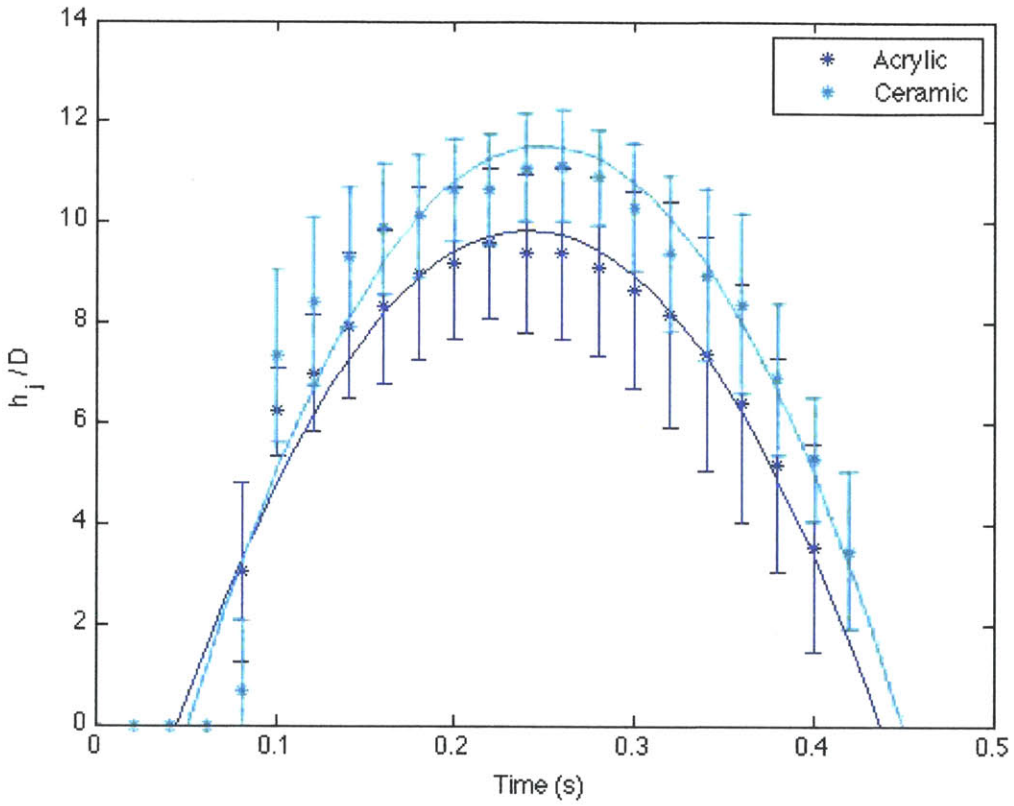

Figure 4-18: Averages of the maximum heights obtained in repeated experiments for the acrylic and ceramic hydrophobic jets at $Fr = 4.86$ are given as a function of time. Error bars indicate one standard deviation above and below the mean. Height of the jet is in normalized by sphere diameter and measures the continuous jet, discounting droplets as they are ejected at the tip.

Qualitatively, Figure 4-18 shows us that the trajectory of the jet tip, on average, is very smooth. However, the parabolic fits to these trajectories do not seem to be the best models for the entire life of the continuous jet. The latter data points appear to follow the ballistic trajectory well, but the initial heights reached by the jet, up until $\sim 20ms$, do not fall along the same ballistic path, but rather move with a higher initial velocity than is represented later. This is readily explained by the fact that the fluid particles tracked at the early instances of the Worthington jet's life break

off from the jet tip very quickly. Therefore the jet tip is likely moving with a much higher velocity than particles that enter the jet later and ultimately form the jet tip as it is measured at the end of the jet's life.

Based on the estimates of experimental error that can be expected in the hydrophobic cases, it is difficult to reach solid conclusions as to the exact model that the Worthington jet's height follows. The general trends that have been pointed out are reasonable estimates of the general behavior, but further, more detailed, studies are necessary to perfect the experiment and obtain more confident results.

4.2.3 Rayleigh-Plateau Instability

An important factor in the breakup of the Worthington jets in the hydrophobic cases is the growth of the Rayleigh-Plateau instability that leads to breakup. From the first moment that the Worthington jet is formed at the pinch-off of the cavity, droplets are breaking off the tip of the jet. Droplets continue to form from the tip throughout the life of the jet, limiting the maximum height that the continuous fluid column reaches. Understanding this process as it applies to the Worthington jet provides valuable insight into the trends in maximum jet heights.

The growth rate of the canonical Rayleigh-Plateau instability, ω, is related to the wavenumber of the disturbance, k, through the dispersion relationship

$$U^2 = \frac{\omega^2}{k^2} = \frac{\sigma}{\rho k R_0^2} \frac{I_1(kR_0)}{I_0(kR_0)} (1 - (kR_0)^2)$$

where U is the local velocity of the jet, R_0 is the radius of the fluid column, usually measured at the stream outlet, I_1 and I_0 are Bessel functions of the first kind, and σ and ρ are the fluid properties. From this well-known relationship, we can extract information about the fastest-growing disturbance mode as it relates to the velocity of the jet tip and the radius of the jet near the tip, which are both measured quantities. Figure 4-19 shows the relationship between these two parameters for all hydrophobic cases. From the dispersion relationship above, it is expected that the velocity of jet tip will be inversely proportional to the radius of the column.

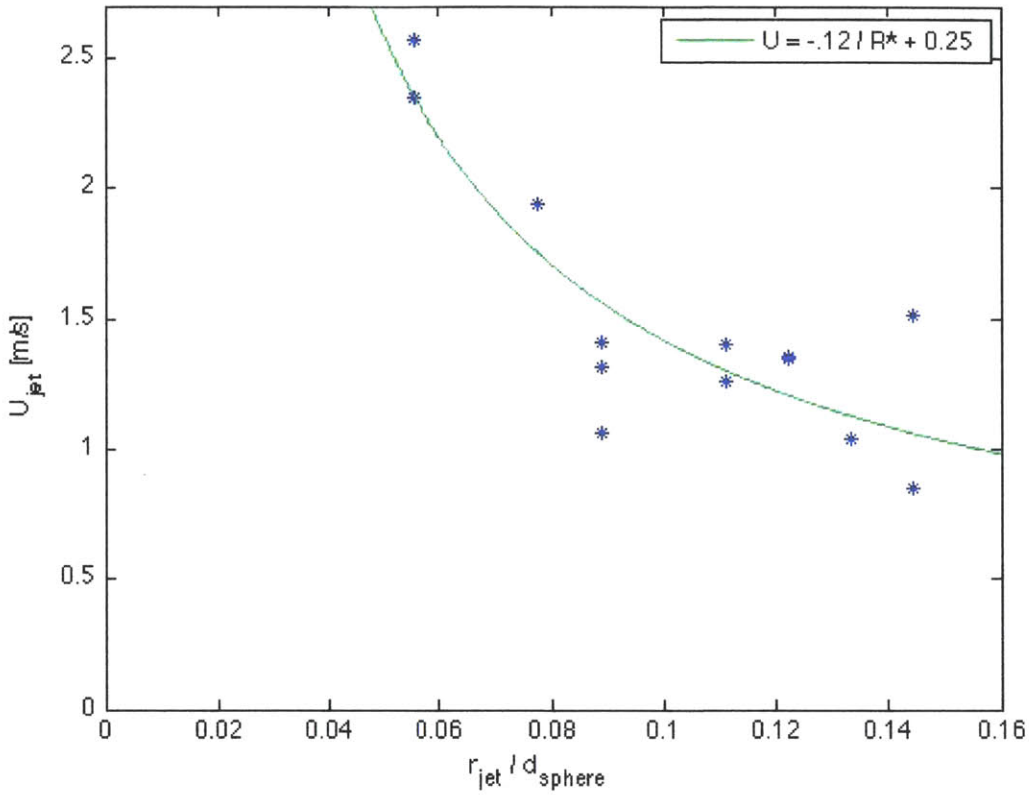

Figure 4-19: The measured velocity of the jet tip is plotted against the non-dimensional radius of the Worthington jet near the tip. The radius is roughly equivalent to the radius parameter used in Rayleigh-Plateau theory, as a constant initial dimension.

The data shows good agreement with the expected relationship. The radius of the jet near the tip is assumed to be a good approximation to the parameter intended by Rayleigh, and is non-dimensionalized by the sphere diameter. The velocity of the jet tip is shown in dimensional form. The agreement with theory provides confidence that the velocity of the jet tip is a good indicator of the behavior of the instability leading to droplet formation at the tip.

Based on the dispersion relationship, it can be shown that the fastest growing mode of the disturbance occurs for $kR_0 = 0.697$. From this, the most relevant disturbance wavenumber can be determined based solely on the measured radius of the Worthington jet. The jet tip velocity is plotted as a function of this minimum wavenumber in Figure 4-20.

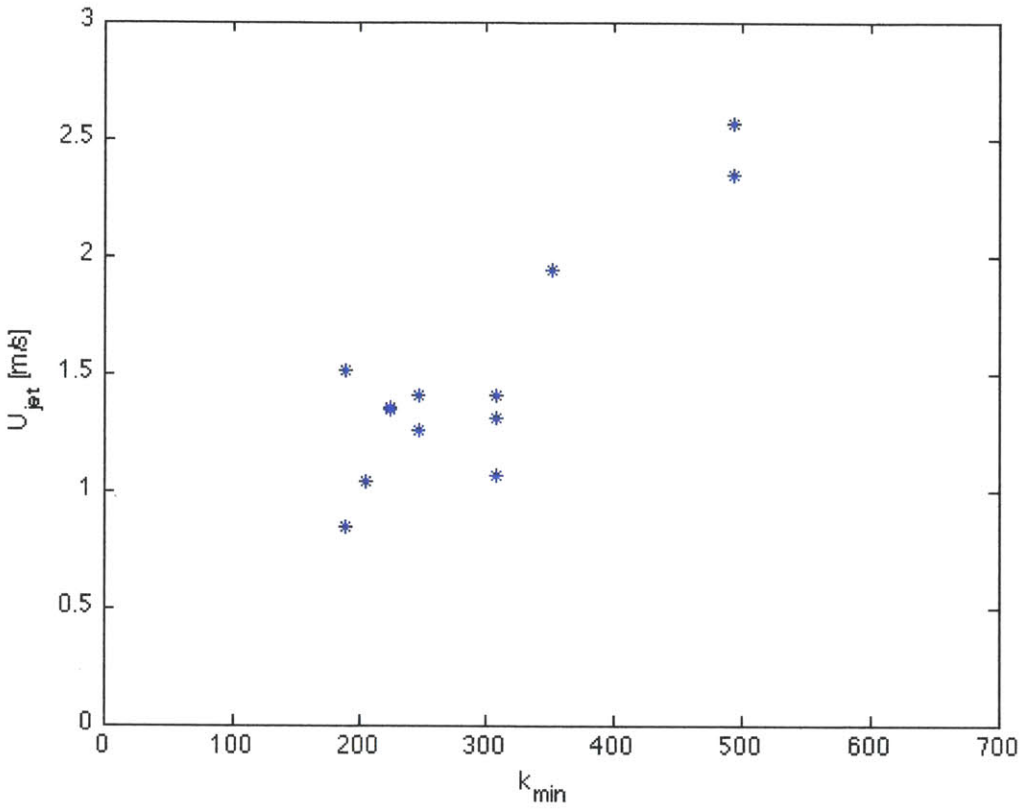

Figure 4-20: The measured velocity of the jet tip is plotted against the wavenumber corresponding to the fastest growing mode obtained from Rayleigh-Plateau theory. The wavenumber is calculated from the radius of the jet near the tip.

Because wavenumber is proportional to the inverse of the jet's radius, it is not surprising that the data in the figure show a linear trend. However, viewing it in this form allows us to better understand the relationship between the local velocity and the breakup-driving instability. As k increases, so does the speed of the perturbation growth, meaning that the disturbance will become more severe more quickly. Figure 4-20 shows that the faster perturbations correspond to faster jets, meaning that faster-travelling Worthington jets will most likely breakup sooner, as would be expected intuitively.

The other key parameter in the dispersion relationship for Rayleigh-Plateau instabilities is the growth rate, ω. This gives direct information about the time to

breakup, which can be estimated by the inverse of the maximum growth rate:

$$t_{breakup} \simeq 2.91\sqrt{\frac{\rho R_0^3}{\sigma}}.$$

This estimate can then be related to the measured maximum average jet height, as shown non-dimensionally in Figure 4-21.

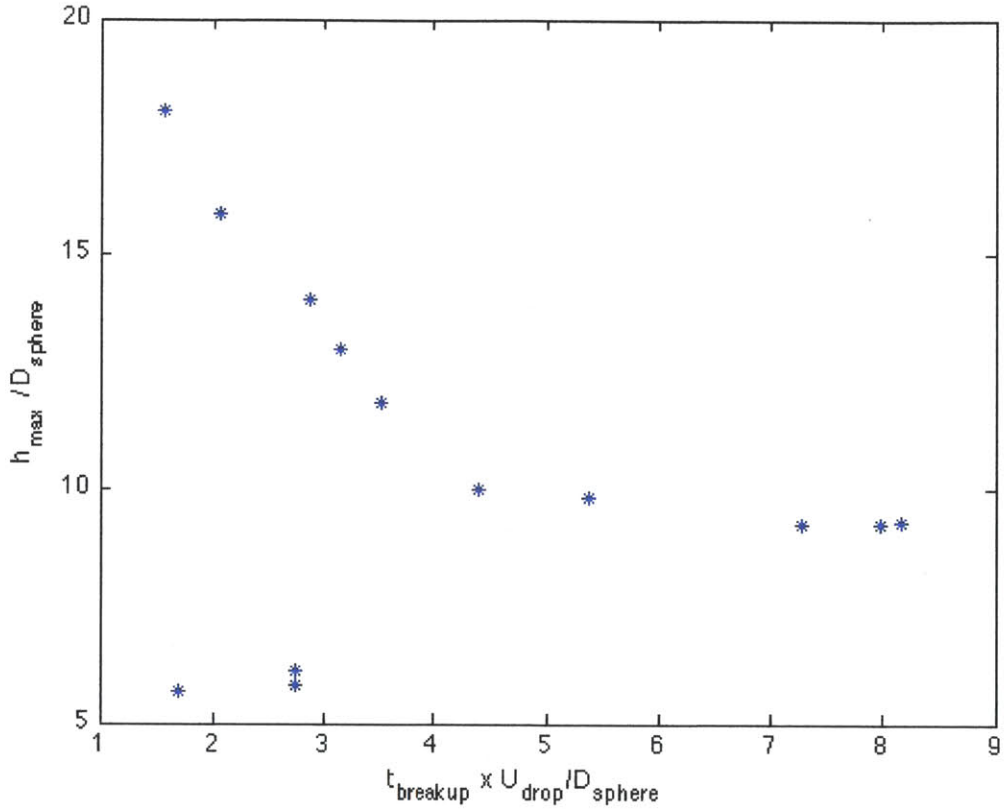

Figure 4-21: The maximum heights of Worthington jets for all hydrophobic cases are plotted against the characteristic breakup time determined by the fastest mode of perturbation growth predicted by Rayleigh-Plateau theory.

The average maximum height is non-dimensionalized by sphere diameter, and the breakup time predicted by Rayleigh-Plateau is non-dimensionalized by the diameter and the velocity of the sphere on impact. When the velocity of the sphere on impact is used, the data collapse into two distinct regimes, as shown in Figure 4-21. For low non-dimensional breakup times, maximum jet height decreases linearly, but above a value of ~ 4, the maximum height is constant. This indicates that although the time

to breakup increases, meaning that it takes longer for droplets to break off from the jet tip, the maximum height of the jet actually decreases, reaching some threshold of minimum height. The three data points that do not fall on the trend are those corresponding to the cases at $Fr = 2.35$, and are obvious outliers.

The main insight gathered from Rayleigh-Plateau is the relationship between the jet radius and velocity and the time to breakup. Jets with larger diameters, which are shown by the dispersion relationship to be slower moving, have faster growing disturbances. These slower jets have longer times to breakup, but because they move slower, reach lower maximum heights. The behavior of the Worthington jet is therefore a balance of jet speed and the breakup process driven by Rayleigh-Plateau. Faster jets can reach greater heights more quickly, but will also break up faster. Slower jets will not form droplets as soon, but will also not travel as far in the same amount of time.

4.2.4 Jet Lifespan

The height of the Worthington jet is not the only parameter of interest. Also measured was the time at which the jet falls back to the free surface. This characteristic is described as fall time, t_f, and is an estimate for the lifetime of the jet. Measured from the time of impact, t_f is the time at which the fluid column is seen to have been overtaken by gravity, and falls back toward the free surface. The indication that this has occurred is quite visible; as the jet reenters the fluid, it entrains air, forming a bubble that is pushed downward from the free surface. Air entrainment occurs in every hydrophobic case.

Normalized fall time is plotted in Figure 4-22 against Fr. The variations in the experiments are not noticeable here, with a very clear linear dependence of t_f^* on Froude number. As with other non-dimensional times, because the impact velocity is included in the terms on both the x and y axes, the dimensional fall time is constant with Froude number. Dependence on mass ratio is almost negligible.

The consistency of the lifespan of the Worthington jets across all of the hydrophobic cases is in great contrast with the variation in maximum heights. Therefore, there

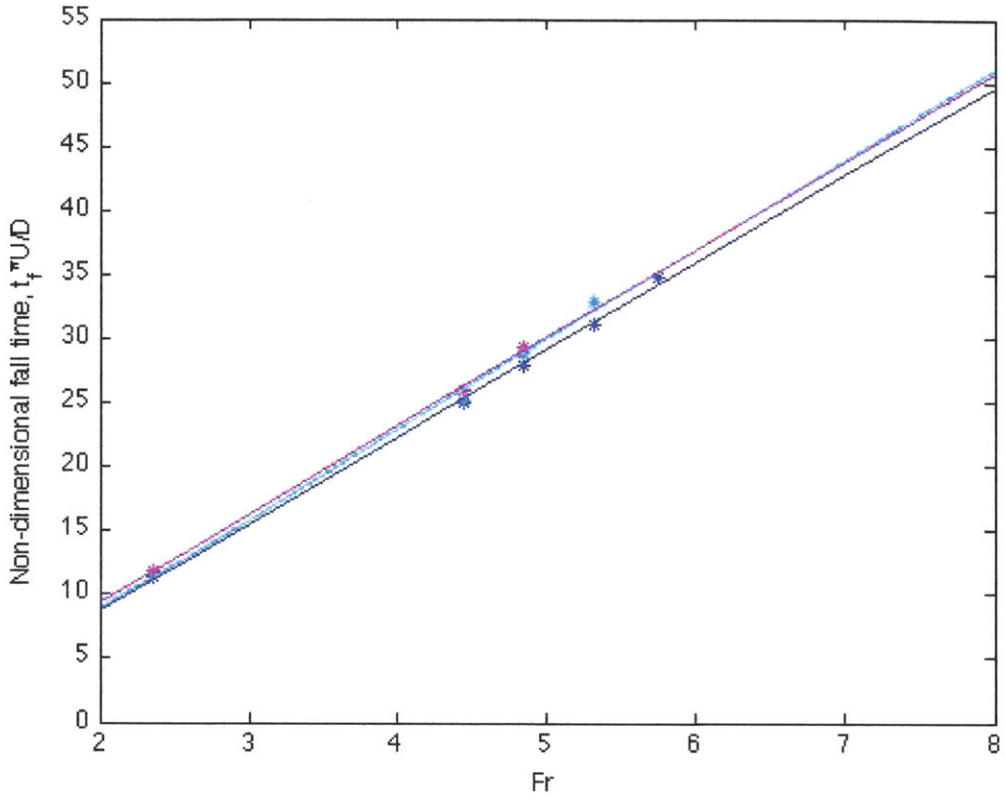

Figure 4-22: The time to the return of the hydrophobic Worthington jet to the free surface, indicated by the bubble of entrained air that descends from the free surface as the jet falls into the fluid, is shown non-dimensionally as a function of Fr. Only hydrophobic cases are shown, and cases in which the jet was not well formed due to the interference of surface closure are not included.

must be a disconnect between the physics that affect the overall formation of the jet and the factors that determine when and where breakup of the tip occurs.

4.2.5 Energy Transfer

As with the hydrophilic cases, it is of interest to find a correlation between the Worthington jet dynamics and the transfer of energy from the sphere to the fluid. In the hydrophobic cases, the most promising source of fluidic energy to feed the Worthington jet is that stored in the cavity. Focusing on the potential energy in the cavity reduces the discrepancy between the energy accounted for and the energy that actually goes into the formation of the Worthington jet.

The potential energy in the cavity stems from the hydrostatic force on the walls from the surrounding fluid. Therefore, the energy can be related to the equivalent buoyant force, F_b of the cavity,

$$F_b = \rho \forall$$

where $\forall$ is the volume of the cavity at pinch-off, measured from raw images.

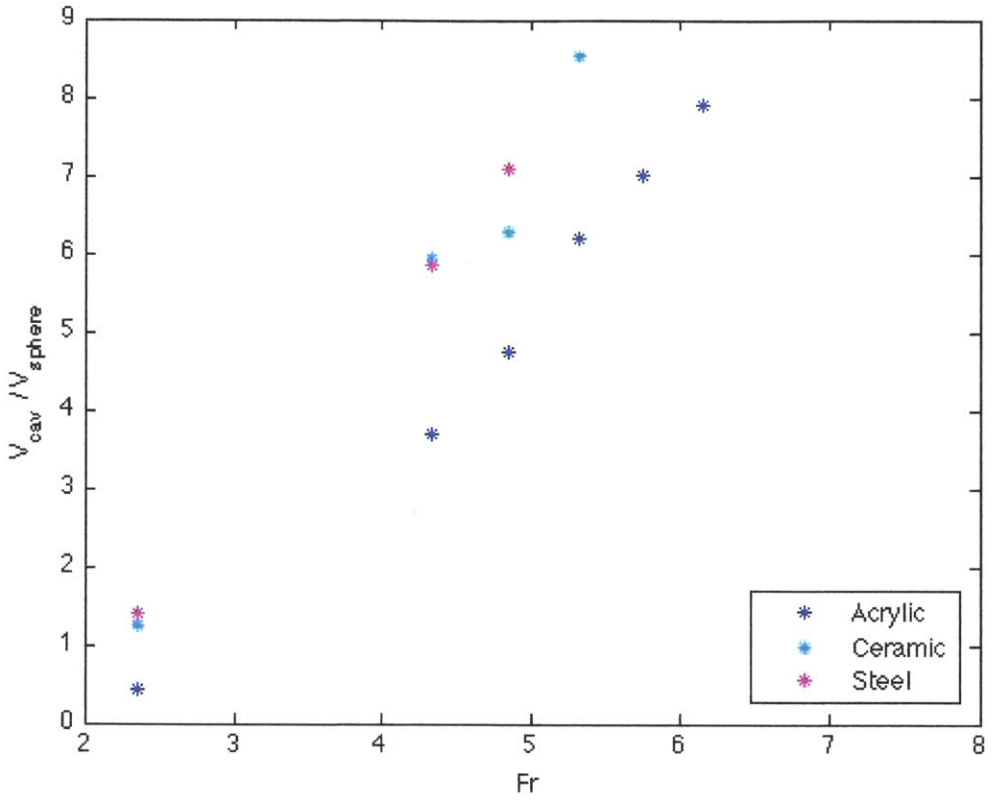

Figure 4-23: Normalized cavity volume is shown as a function of Froude number. There is linear dependence on Fr, and mass ratio is important. The relative contributions of Froude number and mass ratio are not the same as in the case of depth of pinch-off.

The values of the cavity volumes at t_p are plotted against Froude number in Figure 4-23. The volume of the cavity at pinch-off increases proportionally with Froude number, and is also dependent on mass ratio. Due to the transformation of the cavity shape, this dependence on mass ratio differs from the dependence of the depth of pinch-off on m^*. These volumes are used to calculate F_b, and from the

buoyant force, the potential energy of the cavity is then approximated as

$$E_{cav} \approx F_b V_0$$

where V_0 is the velocity of the fluid as it enters the Worthington jet, calculated using the Bernoulli equation as described above.

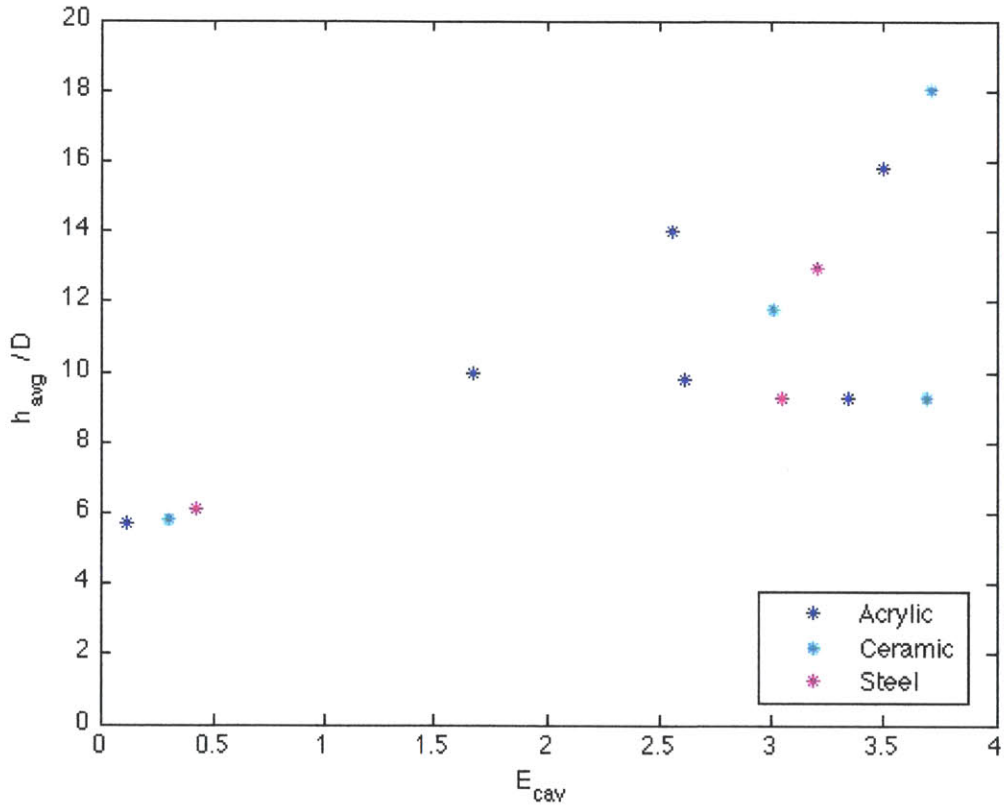

Figure 4-24: Normalized average maximum heights for each case are plotted against the potential energy stored in the cavity. There is a general upward trend in the data, with no evidence of dependence on mass ratio.

To relate the properties of the cavity to the characteristics of the Worthington jet, the jet height is then compared to the values of E_{cav} calculated from the buoyant forces and fluid velocities. This comparison is shown in Figure 4-24. As with other data in the hydrophobic cases, there is a trend, but no concrete organization. As the potential energy of the cavity increases, so does the average maximum height of the Worthington jet, which is expected. However, it is difficult to determine whether the

relationship is linear or follows some other model.

Dependence on mass ratio is once again absent. This has been a constant disconnect between cavity characteristics and the characteristics of the Worthington jet. While mass ratio plays a large role in the formation of the cavity and the location of pinch-off, the dynamics of the fluid following pinch-off rely on other factors. The general correlation between energy in the cavity and the resulting jet height is promising. The error in the hydrophobic experiments is a continuing challenge, but the results seen here still show progress towards scaling laws that fully characterize the Worthington jet.

Chapter 5

Conclusions

Hydrophilic and hydrophobic spheres were dropped from ten heights above the free surface and the resulting Worthington jets were recorded visually at a rate of 500 frames per second. Characteristics of the jets were then analyzed in terms of the Froude and Weber numbers, and trends determined. The values of the Bond and Ohnesorge numbers were also calculated for each case.

5.1 Hydrophilic

In the hydrophilic cases, two separate Worthington jets are formed. The first is formed before the sphere is fully submerged below the free surface, and has a high velocity. The maximum height of this first jet is independent of both Froude number and the mass ratio of the sphere. The time after impact at which the jet breaks up is also independent of mass ratio, but decreases linearly with Fr. The second Worthington jet formed in the hydrophilic cases is much slower, forming after the sphere is submerged. The maximum height of this jet increases linearly with the square of the Froude number, and also increases with increasing mass ratio. The time to breakup of the second jet is independent of both mass ratio and Froude number. The Weber number was calculated from experimental data, and depends on the initial velocity of the fluid as it enters the Worthington jet at the base. The Weber number was found to follow the same trend with respect to Froude number as the maximum

heights of the second jet. This is confirmed by the linear relationship between the maximum height of the second jet and the Weber number. The Bond and Ohnesorge numbers were found to take one value for each jet, as the droplets that are ejected from each jet's tip are uniform in size. Both jets have a value of $Oh \ll 1$, meaning that viscous forces are negligible compared to surface tension forces. The Bond number for the first jet is $\sim O(1)$, and the Bond number for the second jet is $\sim O(10)$. Gravity is therefore important in both jets, but more so in the second. The energy transferred to the fluid by the sphere was calculated from the change in kinetic energy of the sphere from impact to $20ms$ after impact, and was found to increase proportionally to the square of the Froude number with dependence on mass ratio. Spheres of higher mass transfer more energy to the fluid. The height that the second jet reaches, as a result, is linearly proportional to the amount of energy transferred to the fluid by the sphere.

5.2 Hydrophobic

In the hydrophobic cases, much more experimental error was present, clouding the conclusions able to be drawn from the results. Iterations of select cases suggest accuracy of the jet heights to only within two sphere diameters. The Weber number describing the jet has a very weak dependence on the Froude number, and the average maximum height has a vaguely linear dependence on Weber number. Mass ratio of the sphere is not a factor in determining the height characteristics of the jet. The lifespan of the jet, measured as the time from impact to the time at which the jet entrains air on its collapse back to the free surface, is constant for all Froude numbers and mass ratios. The droplets ejected from the Worthington jet are uniform, therefore there is a single value of the Bond and Ohnesorge numbers for the hydrophobic cases. As in the hydrophilic cases, $Oh \ll 1$, so viscous forces are not important. The Bond number is $\sim O(1)$, so gravity is as important as surface tension. The energy ultimately encapsulated in the Worthington jet is thought to scale with the potential energy stored in the cavity walls, equal to the buoyant force of the cavity. The volume

of the cavity at pinch-off increases linearly with Froude number, and has mass ratio dependence. The depth of pinch-off is proportional to $Fr \times m^{*1/4}$, which is not the scaling that the volume of the cavity follows. There is a weak dependence of the height of the Worthington jet on the energy stored in the cavity.

5.3 Future Work

Further work is necessary to clarify the relationships between Worthignton jet characteristics and the dimensionless parameters relevant to the problem. Improvements to the experimental setup might solve some of the measurement inconsistencies, but more focused studies that isolate Weber number as a controllable parameter would also be beneficial. The relationship of the maximum height to the breakup process as described by Rayleigh-Plateau theory also deserves more attention, though the preliminary discussion here is promising. Expanding the results by varying the sphere diameter, adding different materials, and including more Froude numbers would be good improvements to the current data set.

Bibliography

[1] Benjamin Akers and Andrew Belmonte. Impact dynamics of a solid sphere falling into a viscoelastic micellar fluid. *Journal of Non-Newtonian Fluid Mechanics*, 135(2-3):97 – 108, 2006.

[2] Kooichi Utsuno Akira Ogawa and Masatoshi Mutou. Morphological study of cavity and worthington jet formations for newtonian and non-newtonian liquids. *Particulate Science and Technology*, 24:181–225, 2006.

[3] Jeff Aristoff. The water entry of decelerating spheres. *Physics of Fluids*, 2010.

[4] Jeffrey Aristoff and John Bush. Water entry of small hydrophobic spheres. *J of Fluid Mechanics*, 619:45–78, 2009.

[5] Raymond Bergmann, Devaraj van der Meer, Mark Stijnman, Marijn Sandtke, Andrea Prosperetti, and Detlef Lohse. Giant bubble pinch-off. *Phys. Rev. Lett.*, 96(15):154505, Apr 2006.

[6] Garrett Birkhoff, Duncan P. MacDougall, Emerson M. Pugh, and Sir Geoffrey Taylor. Explosives with lined cavities. *Journal of Applied Physics*, 19(6):563–582, 1948.

[7] J. M. Cheny and K. Walters. Extravagant viscoelastic effects in the worthington jet experiment*1. *Journal of Non-Newtonian Fluid Mechanics*, 67:125–135, November 1996.

[8] J. M. Cheny and K. Walters. Rheological influences on the splashing experiment. *Journal of Non-Newtonian Fluid Mechanics*, 86(1-2):185 – 210, 1999.

[9] Minh Do-Quang and Gustav Amberg. The splash of a solid sphere impacting on a liquid surface: Numerical simulation of the influence of wetting. *Physics of Fluids*, 21(2):022102, 2009.

[10] Cyril et al. Duez. Making a splash with water repellency. *Nature Physics*, 2007.

[11] Jens Eggers and Emmanuel Villermaux. Physics of liquid jets. *Reports on Progress in Physics*, 71, 2007.

[12] Alexander I. Fedorchenko and An-Bang Wang. On some common features of drop impact on liquid surfaces. *Physics of Fluids*, 16(5):1349–1365, 2004.

[13] Stephan Gekle and J. M. Gordillo. Generation and breakup of worthington jets after cavity collapse. part 1. jet formation. *Journal of Fluid Mechanics*, 663(-1):293–330, 2010.

[14] Stephan Gekle, José Manuel Gordillo, Devaraj van der Meer, and Detlef Lohse. High-Speed jet formation after solid object impact. *Physical Review Letters*, 102(3), 2009.

[15] D. Gilbarg and R.A. Anderson. Influence of atmospheric pressure on the phenomena accompanying the entry of spheres into water. *J. Applied Physics*, 20(646), 1948.

[16] J. M. Gordillo and Stephan Gekle. Generation and breakup of worthington jets after cavity collapse. part 2. tip breakup of stretched jets. *Journal of Fluid Mechanics*, 663(-1):331–346, 2010.

[17] Jakum Kominiarczuk Hongmei Yan, Yuming Liu and Dick KP Yue. Cavity dynamics in water entry at low froude numbers. *J of Fluid Mechanics*, 641:441–461, 2009.

[18] Mingying Hsiao, Seth Lichter, and Luis G. Quintero. The critical weber number for vortex and jet formation for drops impinging on a liquid pool. *Physics of Fluids*, 31(12):3560–3562, 1988.

[19] M. Lee. On the water-entry-induced cavity closure for a wide range of entry speeds. *Journal of Fluids Engineering*, 125(5):927–930, 2003.

[20] Detlef et al. Lohse. Impact on soft sand: Void collapse and jet formation. *Physical Review Letters*, 93(19):198003, 2004.

[21] F.R.S. Lord Rayleigh. On the instability of jets. *Proc. London Math Society*, 4(13), 1878.

[22] R.G. Longoria M. Lee and D.E. Wilson. Cavity dynamics in high-speed water entry. *Physics of Fluids*, 1997.

[23] J. O. MARSTON and S. T. THORODDSEN. Apex jets from impacting drops. *Journal of Fluid Mechanics*, 614(-1):293–302, 2008.

[24] A. May. Vertical entry of missiles into water. *J. Applied Physics*, 23(1362), 1952.

[25] M. Moghisi and P. T. Squire. An experimental investigation of the initial force of impact on a sphere striking a liquid surface. *Journal of Fluid Mechanics Digital Archive*, 108(-1):133–146, 1981.

[26] S. Nigen and K. Walters. On the two-dimensional splashing experiment for newtonian and slightly elastic liquids. *Journal of Non-Newtonian Fluid Mechanics*, 97(2-3):233 – 250, 2001.

[27] E G Richardson. The impact of a solid on a liquid surface. *Proceedings of the Physical Society*, 61(4):352–367, 1948.

[28] John R. Royer, Eric I. Corwin, Andrew Flior, Maria-Luisa Cordero, Mark L. Rivers, Peter J. Eng, and Heinrich M. Jaeger. Formation of granular jets observed by high-speed x-ray radiography. *Nat Phys*, 1(3):164–167, December 2005.

[29] Jordan Shin and Thomas A McMahon. The tuning of a splash. *Physics of Fluids*, 2(8):1312–1317, August 1990.

[30] S. T. Thoroddsen and Amy Q. Shen. Granular jets. *Physics of Fluids*, 13(1):4, 2001.

[31] TT Truscott and Alexandra H. Techet. Water entry of spinning spheres. *J of Fluid Mechanics*, 625:125–165, 2009.

[32] Walters. The competing roles of extensional viscosity and normal stress differences in complex flows of elastic liquids. *Korea-Australia Rheology Journal*, 21(4):225–233, December 2009.

[33] A. M. Worthington. On impact with a liquid surface. *Proceedings of the Royal Society of London*, 34:217–230, 1882.

[34] A.M. Worthington. Impact with a liquid surface studied by the aid of instantaneous photography. *Philosophical Transactions of the Royal Society of London*, 194:175–199, 1899.

[35] A.L. Yarin. Drop impact dynamics: Splashing, spreading, receding, bouncing... *Annual Review of Fluid Mechanics*, 38:159–192, 2006.

[36] Benjamin W. Zeff, Benjamin Kleber, Jay Fineberg, and Daniel P. Lathrop. Singularity dynamics in curvature collapse and jet eruption on a fluid surface. *Nature*, 403(6768):401–404, 01 2000.